Effect of Unsteady Surface Water Hydraulics on Mixing-Dependent Hyporheic Denitrification in Riverbed Dunes

Lauren A. Eastes

Thesis submitted to the faculty of the Virginia Polytechnic Institute and State University in partial fulfillment of the requirements for the degree of

Master of Science In Environmental Engineering

Erich T. Hester, Chair

Mark A. Widdowson

Madeline E. Schreiber

June 1, 2018

Blacksburg, VA

Keywords: hyporheic, surface water-groundwater exchange, transient, pollutant attenuation, nitrate, denitrification, streams, rivers, contaminants, sediments

Effect of Unsteady Surface Water Hydraulics on Mixing-Dependent Hyporheic Denitrification in Riverbed Dunes

Lauren Eastes

ABSTRACT

Increased reactive nitrogen from human activities negatively affects surface water (SW) quality. The hyporheic zone, where SW and groundwater interact, possesses unique biogeochemical conditions that can attenuate contaminants (e.g., denitrification), including mixing-dependent reactions that require components from both water sources. Previous research has explored mixing-dependent denitrification in the hyporheic zone but did not address the effects of varying SW depth as would occur from storms, tides, dam operation, and varying seasons. We simulated steady and unsteady hyporheic flow and transport through a riverbed dune using MODFLOW and SEAM3D, and varied SW depth, degree of sediment heterogeneity, amplitude and frequency of sinusoidal fluctuations, among others to determine these effects. We found that increasing steady state surface water depth from 0.1 to 1.0 m increased non-mixing dependent aerobic respiration by 270% and mixing-dependent denitrification by 78% in homogeneous sediment. Heterogeneous hydraulic conductivity fields yielded similar results, with increases in consumption due to variation in correlation length and variance of less than 5%. Daily SW fluctuation, including variation of amplitude, period, and sinusoidal versus instantaneous changes had significantly less impact than longer-term trends in SW depth. There is potential for the hyporheic zone to attenuate NO_3^- in upwelling groundwater plumes. Restoration efforts may be able to maximize the potential for mixing-dependent reactions in the hyporheic zone by increasing residence times.

Effect of Unsteady Surface Water Hydraulics on Mixing-Dependent Hyporheic Denitrification in Riverbed Dunes

Lauren Eastes

GENERAL AUDIENCE ABSTRACT

Increased nitrogen in runoff from human activities negatively affects surface water quality. The hyporheic zone is where surface water and groundwater interact, and the mixing between the waters can help to this nitrogen to undergo reaction (denitrification), potentially stopping the contaminant from spreading. Previous research has explored this idea, but has not addressed the impact of varying surface water depth, as would realistically occur due to storms, tides, dam operation, and varying seasons. We simulated both constant and fluctuating surface water conditions on a riverbed dune to see the effects on hyporheic flow and denitrification. Test variables included the surface water depth, the degree of sediment heterogeneity, the amplitude and frequency of surface water fluctuations. We found that increasing the steady-state surface water depth had the most dramatic increase on the amount of reaction undergone. This trend was also seen in heterogeneous sediment. Any daily-scale surface water fluctuations, including runs that varied the amplitude, period, and sinusoidal vs instantaneous changes in surface water depth, had significantly less impact than longer-term trends in surface water depth.

Acknowledgements

I would like to thank Dr. Erich Hester and Dr. Mark Widdowson for their invaluable guidance and support while completing my thesis. A special thanks to Dr. Mark Widdowson for his assistance with troubleshooting the model development in MODFLOW and SEAM3D. I would also like to thank both Morgan Dicarlo and Carlos Mantilla Peña for assisting me in using R. Additionally, I thank my family, friends, and research group for all of their support. Finally, I would like to thank Dr. Madeline Schreiber for joining my committee.

Table of Contents

List of Figures

List of Tables

List of Abbreviations

DOC	Dissolved organic carbon
DO	Dissolved oxygen
GMS	Groundwater Model Software
SW	Surface water
K_{xx}	Value of hydraulic conductivity along the x coordinate axis
K_{yy}	Value of hydraulic conductivity along the y coordinate axis
K_{zz}	Value of hydraulic conductivity along the z coordinate axis
h	Potentiometric head
W	Volumetric flux per until volume representing sources and/or sinks of water
S_s	Specific storage of the porous media
t	Time
θ	Porosity of the subsurface medium
C^k	Dissolved concentration of species *k*
$x_{i,j}$	Distance along Cartesian coordinate axis
$D_{i,j}$	Hydrodynamic dispersion coefficient tensor
$v_{i,j}$	Linear pore water velocity
R_k	Reaction term
M_n	Biomass concentration for reaction *n*
M_{AR}	Biomass concentration for aerobic respiration
M_{DN}	Biomass concentration for denitrification
$\gamma_{n,k}$	Use coefficient of subspecies *k* for reaction *n*
$\gamma_{DO,AR}$	Use coefficient of DO for aerobic respiration
$\gamma_{NO_3^-,DN}$	Use coefficient of NO_3^- for denitrification
v_n	The maximum specific rate of utilization for reaction *n*
v_{AR}	The maximum specific rate of utilization for aerobic respiration
v_{DN}	The maximum specific rate of utilization for denitrification
C_{ED}	Electron donor (DOC) concentration
C_{EA}	Electron acceptor concentration
C_{DOC}	DOC concentration
C_{DO}	DO concentration
$C_{NO_3^-}$	NO_3^- concentration
K_{ED}	Half saturation constant for the electron donor
K_{EA}	Half saturation constant for the electron acceptor
K_{DOC}	Half saturation constant for DOC
K_{DO}	Half saturation constant for DO
$K_{NO_3^-}$	Half saturation constant for NO_3^-
I	Inhibition function
K_I	Inhibition constant for denitrification
d	Time-dependent mean flow depth of the surface water defined as depth above the bedform crest plus half of the bedform height
A	Amplitude of the fluctuation
P	Period of the fluctuation
d_{avg}	Average depth of the surface water across time
U	Surface water velocity

S	Channel slope
n	Manning's coefficient
h_m	half of the amplitude of the variation in $h_{dynamic}$
$h_{dynamic}$	dynamic head at the bed surface
H	height of the dune
H/d	Relative roughness
$h_{surface}$	actual surface water head

1.0 Introduction

1.1 Literature Review

The hyporheic zone is an area of exchange between surface water and groundwater within the sediment of streams and estuaries [*Brunke and Gonser*, 1997; *Harvey and Wagner*, 2000, *White*, 1993]. Hyporheic exchange can be driven by many hydrologic factors. Flow can be hydrostatically driven (e.g. by obstructions of flow, either natural in the case of logs and boulders or anthropogenic in the case of weirs or dams [*Hester et al.*, 2008; *Winter et al*., 1998]; by pool-riffle sequences [*Saenger et al.*, 2005; *Storey et al.*, 2003; *Tonina and Buffington*, 2011]) or form drag driven (e.g. by surface flow over rough riverbed morphological forms such as dunes and ripples [*Elliott and Brooks*, 1997a,b; *Packman*, 2004], by larger-scale morphological forms such as cascades and meanders [*Cardenas*, 2009a]). In all cases, a hydraulic gradient allows bidirectional flow through the riverbed, where the surface water enters the subsurface then reenters the surface water flow [*White*, 1993; *Winter et al.*, 1998]. As a result of its unique biogeochemical properties, the hyporheic zone often facilitates certain reactions and microbial processes, including denitrification [*Duff and Triska*, 1990; *Hill and Lymburner*, 1998; *Triska et al.*, 1989; *Winter*, 1993; *Zarnetske et al.*, 2011].

1.1.1 Reactions in the hyporheic zone

The unique biogeochemical makeup of the hyporheic zone provides a reaction site for many contaminants that otherwise would not be attenuated. The hyporheic zone allows the mixing of reactants from different source waters, enabling many different reactions to take place, including attenuation of compounds like PCE [*Conant et al.*, 2004], MTBE, TBA, and TAME [*Landmeyer et al.*, 2010]; heavy metals like Cr(VI) [*Moser et al.*, 2003]; and nitrate [*Kennedy et al.*, 2009]. Denitrification is a particularly important reaction performed in the hyporheic zone [*Duff and Triska*, 1990; *Gomez-Valez et al.*, 2015; *Hill and Lymburner*, 1998; *Triska et al.*, 1989; *Zarnetske*, 2011]. Reactive nitrogen sourced from runoff into surface water from agricultural runoff and sewage from humans and livestock [*Braun*, 2007] can be converted from NO_3^- to unreactive N_2 if the aquifer is anoxic and contains labile dissolved organic carbon (DOC) [*Spanning et al*., 2008].

1.1.1.2 Non-mixing dependent reaction

Non-mixing dependent reactions are characterized by sourcing all reactants from the same source water and not requiring intermixing among source waters in order to occur. For non-mixing dependent reactions, either all reactants come from the surface water or the groundwater and travel along the same flowpaths. The majority of the current literature discussing reactions in the hyporheic zone focuses on quantifying non-mixing dependent reactions of contaminants. This includes studies on nitrification [*Jones et al.*, 1995; *Zarnetske*, 2011] and the attenuation of compounds like toluene [*Kim et al.*, 1995]. Most papers quantifying denitrification do not separate out the amount of mixing-dependent reaction happening in the hyporheic zone [*Bardini et al.*, 2012; *Boano et al.*, 2010; *Harvey et al.*, 2013; *Zarnetske*, 2012].

1.1.1.2 Mixing-dependent reaction

Some reactions occur specifically due to the mixing of the surface water and groundwater. These mixing-dependent reactions have reactants that originate from both source waters. The idea of mixing-dependent reactions has mostly been explored in deeper aquifer studies, where contaminant plumes in groundwater, including toluene and nitrate [*Bauer et al.*, 2009], are attenuated at the fringe of the plume [*Bauer et al.*, 2009; *Castro-Alcalá et al.*, 2012; *Cirpka et al.*, 1999]. While these studies have explored mixing-dependent reactions, very few hyporheic studies [*Hester et al.*, 2013; *Hester et al.*, 2014; *Naranjo*, 2015] have focused on a mixing-dependent reaction mechanism. In terms of the hyporheic zone, mixing-dependent reactions occur when some of the reactants come from the downwelling surface water and mix with reactants in the upwelling groundwater.

1.1.2 Hydraulic fluctuations

1.1.2.1 Sources of fluctuations in surface water

There are many reasons that river stage may fluctuate, at times dramatically. Some hydrological causes of these unsteady conditions are discussed below.

Storms are a pulse event for rivers and can sharply increase river stage over a period ranging several hours [*Hopkinson and Walburn*, 2015] to a couple of days [*Dudley-Southern and Binley, 2015; Malzone et al., 2016*]. A rapidly rising river stage can lead to reversal of vertical hydraulic gradients. In a gaining river, a rapid rise in stage can even generate downwelling

conditions and induce hyporheic exchange [*Dudley-Southern and Binley*, 2015]. Fluctuations in river stage control two competing processes. The first is an increase in the volume of surface water entering the bed as stage rapidly increases; the second is an increase in the hydraulic gradient toward the river as precipitation recharges the underlying aquifer, compressing the hyporheic zone. These two processes are the competing elements that storm surges induce [*Zimmer and Lautz*, 2014].

Many sources of river stage fluctuation, including snowmelt [*Loheide and Lundquist*, 2009], tidal cycles [*Bianchin et al.*, 2011; *Pool et al.*, 2014; *Pool et al.*, 2015], dam operations [*Sawyer et al.*, 2009] and evapotranspiration [*McCallum and Shanafield*, 2016; *Schmadel et al.*, 2016], fluctuate on a diel scale. These fluctuations can alter and even induce hyporheic exchange spanning over three orders of magnitude [*Schmadel et al.*, 2016]. While storms occur as pulse events, diel fluctuations are regular and cyclical in their occurrence. They are often modelled as a sinusoidal curve [*Huang et al.*, 2015; *McCallum and Shanafield*, 2016; *Pool*, 2014; *Pool*, 2015].

Hydropeaking refers to the daily "pulses" of increased river flow often emitted from hydroelectric dams. These lead to large, rapid fluctuations in the water table and a laterally expanded hyporheic zone, as well as flow directions that regularly reverse [*Arntzen et al.*, 2006; *Casas-Mulet et al.*, 2015; *Sawyer et al.*, 2009]. Streams and rivers near coastlines may still be affected by the tides. However, the severity of the effect is greatly influenced by the distance from the coast; moving further inland damps the tidally-induced surface water perturbation seen [*Huang et al.*, 2015]. Snowmelt also acts on a diel cycle as more melts during the warmer days than the cooler nights. This is seen in both the water table and the river stage [*Loheide and Lundquist*, 2009].

1.1.2.2 Sources of fluctuations in groundwater

Upwelling groundwater has a significant impact on the amount of hyporheic exchange occurring in a system. Increased upwelling limits the amount of surface water infiltrating the riverbed [*Cardenas*, 2009b; *Dudley-Southern and Binley*, 2015; *Hester et al.*, 2008].

In the case of storm events, the groundwater response is typically longer-term and can potentially occur out-of-phase with the surface water response and moderate the peak [*Malzone et al.*, 2016].

The antecedent conditions such as moisture, geomorphology, geology, and catchment structure also heavily influence the fluctuations seen in the size and depth of the hyporheic zone. As a result, the time of year is also very important for determining groundwater response [*Fitts*, 2013]; if the background discharge is high, the hyporheic zone will undergo less expansion in a storm [*Malzone et al.*, 2016]. The water table fluctuates on a seasonal scale, typically declining in summer months to a minimum level in fall due to increased evapotranspiration from both the trees and warmer air. Evapotranspiration is at a minimum during the winter months due to the colder air, and the groundwater table can then recharge until reaching a peak in spring due to snowmelt [*Fitts*, 2013].

1.1.2.3 Effect of fluctuations on hyporheic reactions

These fluctuations are important for the biogeochemistry of the stream; they have been shown to remove nitrates [*Gu et al.*, 2012], preserve the natural stream chemistry [*McCallum et al.*, 2010], allow heat transport [*Anderson et al.*, 2011], retard the movement of stream solutes [*Lin and Medina*, 2003], and even prevent solutes from reaching the stream altogether [*Squillace et al.*, 1993; *Squillace*, 1996]. Unsteady models have shown that increasing the amplitude of fluctuations in river stage produces longer flow paths and residence times [*Schmadel et al.*, 2016], although observed hyporheic exchange data from storm events only slightly increases the mixing depth of surface water and groundwater [*Dudley-Southern and Binley*, 2015].

Previous work has observed mixing dependent reactions in the hyporheic zone [*Hester et al.*, 2013] and the effects of heterogeneity [*Hester et al.*, 2014]. However, not much is known of the effects of unsteady surface water head conditions on these reactions. The purpose of this study is to observe and quantify these effects and ultimately determine the potential effects of fluctuating river stage conditions on hyporheic exchange and the resulting mixing-dependent reactions that may occur.

1.1.3 Purpose of study

Hyporheic flow cells create mixing between downwelling surface water and upwelling groundwater. This exchange may be driven by riverbed morphology through hydrostatic head variations and form drag [*Elliott and Brooks*, 1997a,b; *Hester and Doyle*, 2008; *Sawyer et al.*, 2011]. At the interface of the surface water and groundwater, a thin mixing zone develops and allows mixing-dependent reactions (e.g. denitrification) to occur. In this study, we used

numerical modeling to quantify denitrification in the hyporheic mixing zone of a riverbed dune of a gaining river. Similar bedforms are commonly found in medium to large waterways, and the hydraulics of these have been well-studied [*Cardenas and Wilson*, 2007; *Elliott and Brooks*, 1997a,b; *Sinha*, 2017]. The objectives of this study are to:

1. Quantify the effects of differing surface water depths on mixing-dependent denitrification in the system.
2. Quantify the effects of unsteady, oscillating surface water depth conditions on the amount of denitrification in the system and the effect on the percentage of reactants that are consumed.
3. Determine how differing surface water depths interact with other variables, including heterogeneity.

1.2 Organization of thesis

This thesis is organized in a manuscript format. Section 2 contains a journal article that will likely be submitted for publication in *Water Resources Research.* The introduction of this article (Section 2.1) is a condensed version of the literature review in this section. Section 3 contains engineering applications and the significance of the study. The discussion contains in Section 2.4.2 contains an abbreviated version of Section 3. The Appendix contains all supporting material, including additional figures and plots, as well as more detailed methodology.

References

Anderson, W. P., Storniolo, R. E., & Rice, J. S. (2011). Bank thermal storage as a sink of temperature surges in urbanized streams. *Journal of Hydrology*, *409*(1–2), 525–537. https://doi.org/10.1016/j.jhydrol.2011.08.059

Arntzen, E. V., D. R. Geist, and P. E. Dresel. 2006. Effects of fluctuating river flow on groundwater/surface water mixing in the hyporheic zone of a regulated, large cobble bed river. River Research and Applications 22:937-946

Bardini, L., Boano, F., Cardenas, M. B., Revelli, R., & Ridolfi, L. (2012). Nutrient cycling in bedform induced hyporheic zones. *Geochimica et Cosmochimica Acta*, *84*, 47–61. https://doi.org/10.1016/j.gca.2012.01.025

Bauer, R. D., Rolle, M., Bauer, S., Eberhardt, C., Grathwohl, P., Kolditz, O., Griebler, C. (2009). Enhanced biodegradation by hydraulic heterogeneities in petroleum hydrocarbon plumes. *Journal of Contaminant Hydrology*, *105*(1–2), 56–68. https://doi.org/10.1016/j.jconhyd.2008.11.004

Bianchin, M. S., L. Smith, and R. D. Beckie. 2011. Defining the hyporheic zone in a large tidally influenced river. Journal of Hydrology 406:16-29.

Boano, F., Demaria, A., Revelli, R., & Ridolfi, L. (2010). Biogeochemical zonation due to intrameander hyporheic flow. *Water Resources Research*, *46*(2), 1–13. https://doi.org/10.1029/2008WR007583

Braun, E. (2007). *Reactive nitrogen in the environment: too much or too little of a good thing.* Paris; Falmouth, MA: UNEP DTIE, Sustainable Consumption and Production (SCP) Branch ; Woods Hole Research Center.

Brunke, M., & Gonser, T. (1997). The ecological significance of exchange processes between rivers and groundwater. *Freshwater Biology*, *37*(1), 1–33. https://doi.org/10.1046/j.1365-2427.1997.00143.x

Cardenas, M. B. (2009). A model for lateral hyporheic flow based on valley slope and channel sinuosity. *Water Resources Research*, *45*(1), 1–5. https://doi.org/10.1029/2008WR007442

Cardenas, M. B. (2009). Stream-aquifer interactions and hyporheic exchange in gaining and losing sinuous streams. *Water Resources Research*, *45*(6), 1–13. https://doi.org/10.1029/2008WR007651

Cardenas, M. B., & Wilson, J. L. (2007). Hydrodynamics of coupled flow above and below a sediment-water interface with triangular bedforms. *Advances in Water Resources*, *30*(3), 301–313. https://doi.org/10.1016/j.advwatres.2006.06.009

Casas-Mulet, R., Alfredsen, K., Hamududu, B., & Timalsina, N. P. (2015). The effects of hydropeaking on hyporheic interactions based on field experiments THE EFFECT OF HYDROPEAKING ON HYPORHEIC INTERACTIONS John Wiley & Sons Inc. doi:10.1002/hyp.10264

Castro-Alcalá, E., Fernaàndez-Garcia, D., Carrera, J., & Bolster, D. (2012). Visualization of mixing processes in a heterogeneous sand box aquifer. *Environmental Science and Technology*, *46*(6), 3228–3235. https://doi.org/10.1021/es201779p

Cirpka, O. A., Frind, E. O., & Helmig, R. (1999). Numerical simulation of biodegradation controlled by transverse mixing. *Journal of Contaminant Hydrology*, *40*(2), 159–182. https://doi.org/10.1016/S0169-7722(99)00044-3

Conant, B., J. A. Cherry, and R. W. Gillham. 2004. A PCE groundwater plume discharging to a river: influence of the streambed and near-river zone on contaminant distributions. Journal of Contaminant Hydrology 73:249-279.

Dudley-Southern, M., & Binley, A. (2015). Temporal responses of groundwater-surface water exchange to successive storm events. *Water Resources Research*, *51*(2), 1112–1126. https://doi.org/10.1002/2014WR016623

Duff, J. H., & Triska, F. J. (1990). Denitrification in sediments from the hyporheic zone adjacent to a small forested stream. *Canadian Journal of Fisheries and Aquatic Sciences*, *47*(6), 1140–1147. https://doi.org/10.1139/f90-133

Elliott, H., & Brooks, N. H. (1997). Transfer of nonsorbing solutes to a streambed with bed forms : Theory. *Water Resources Research*, *33*(1), 123–136.

Elliott, H., & Brooks, N. H. (1997). Transfer of nonsorbing solutes to a streambed with bed forms: Laboratory experiments. *Water Resources Research*, *33*(1), 137–151.

Fitts, Charles R. (2013) *Groundwater Science (Second Edition)*, Boston: Academic Press. https://doi.org/10.1016/B978-0-12-384705-8.00001-7.

Gomez-Velez, J. D., Harvey, J. W., Cardenas, M. B., & Kiel, B. (2015). Denitrification in the Mississippi River network controlled by flow through river bedforms. *Nature Geoscience*, *8*(12), 941–945. https://doi.org/10.1038/ngeo2567

Gu, C., Anderson, W., & Maggi, F. (2012). Riparian biogeochemical hot moments induced by stream fluctuations. *Water Resources Research*, *48*(9), 1–17. https://doi.org/10.1029/2011WR011720

Harvey, J. W., Böhlke, J. K., Voytek, M. A., Scott, D., & Tobias, C. R. (2013). Hyporheic zone denitrification: Controls on effective reaction depth and contribution to whole-stream mass balance. *Water Resources Research*, *49*(10), 6298–6316. https://doi.org/10.1002/wrcr.20492

Hester, E. T., Young, K. I., & Widdowson, M. A. (2013). Mixing of surface and groundwater induced by riverbed dunes: Implications for hyporheic zone definitions and pollutant reactions. *Water Resources Research*, *49*(9), 5221–5237. https://doi.org/10.1002/wrcr.20399

Hester, E. T., & Doyle, M. W. (2008). In-stream geomorphic structures as drivers of hyporheic exchange. *Water Resources Research*, *44*(3). https://doi.org/10.1029/2006WR005810

Hester, E. T., Young, K. I., & Widdowson, M. A. (2014). Controls on mixing-dependent denitrification in hyporheic zones induced by riverbed dunes: A steady state modeling study. *Water Resources Research*, *50*(11), 9048–9066. https://doi.org/10.1002/2014WR015424

Hill, A. R., & Lymburner, J. (1998). Hyporheic zone chemistry and stream-subsurface exchange in two groundwater-fed streams. *Canadian Journal of Fisheries and Aquatic Sciences*, *55*(1996), 495–506. https://doi.org/10.1139/f97-250

Hopkinson, L. C., & Walburn, C. Z. (2016). Near-boundary velocity and turbulence in depth-varying stream flows. *Environmental Fluid Mechanics*, *16*(3), 559–574. https://doi.org/10.1007/s10652-015-9440-1

Huang, F. K., Chuang, M. H., Wang, G. S., & Yeh, H. Der. (2015). Tide-induced groundwater level fluctuation in a U-shaped coastal aquifer. *Journal of Hydrology*, *530*, 291–305. https://doi.org/10.1016/j.jhydrol.2015.09.032

Jones, J. B., S. G. Fisher, and N. B. Grimm. 1995. Nitrification in the Hyporheic Zone of a Desert Stream Ecosystem. Journal of the North American Benthological Society 14:249-258.

Kennedy, C. D., D. P. Genereux, D. R. Corbett, and H. Mitasova. 2009. Relationships among groundwater age, denitrification, and the coupled groundwater and nitrogen fluxes through a streambed. Water Resources Research 45:W09402.

Kim, H. K., H. F. Hemond, L. R. Krumholz, and B. A. Cohen. 1995. In-situ biodegradation of toluene in a contaminated stream. 1. Field studies. Environmental Science & Technology 29:108-116

Landmeyer, J. E., P. M. Bradley, D. A. Trego, K. G. Hale, and J. E. Haas. 2010. MTBE, TBA, and TAME Attenuation in Diverse Hyporheic Zones. Ground Water 48:30-41.

Lin, Y. C., & Medina, M. A. (2003). Incorporating transient storage in conjunctive stream-aquifer modeling. *Advances in Water Resources*, *26*(9), 1001–1019. https://doi.org/10.1016/S0309-1708(03)00081-2

Loheide, S. P., & Lundquist, J. D. (2009). Snowmelt-induced diel fluxes through the hyporheic zone. *Water Resources Research*, *45*(7), 1–9. https://doi.org/10.1029/2008WR007329

Malzone, J. M., Lowry, C. S., & Ward, A. S. (2016). Response of the hyporheic zone to transient groundwater fluctuations on the annual and storm event time scales. *Water Resources Research*, *52*(7), 5301–5321. https://doi.org/10.1002/2015WR018056

McCallum, J. L., Cook, P. G., Brunner, P., & Berhane, D. (2010). Solute dynamics during bank storage flows and implications for chemical base flow separation. *Water Resources Research*, *46*(7), 1–12. https://doi.org/10.1029/2009WR008539

McCallum, J. L., & Shanafield, M. (2016). Residence times of stream-groundwater exchanges due to transient stream stage fluctuations. *Water Resources Research*, *52*(3), 2059–2073. https://doi.org/10.1002/2015WR017441

Moser, D. P., J. K. Fredrickson, D. R. Geist, E. V. Arntzen, A. D. Peacock, S. M. W. Li, T. Spadoni, and J. P. McKinley. 2003. Biogeochemical processes and microbial characteristics across groundwater-surface water boundaries of the Hanford Reach of the Columbia River. Environmental Science & Technology 37:5127-513

Packman, A. I., Salehin, M., & Zaramella, M. (2004). Hyporheic Exchange with Gravel Beds: Basic Hydrodynamic Interactions and Bedform-Induced Advective Flows. *Journal of Hydraulic Engineering*, *130*(7), 647–656. https://doi.org/10.1061/(ASCE)0733-9429(2004)130:7(647)

Peralta-Maraver, I., Reiss, J., & Robertson, A. L. (2018). Interplay of hydrology, community ecology and pollutant attenuation in the hyporheic zone. *Science of the Total Environment*, *610–611*, 267–275. https://doi.org/10.1016/j.scitotenv.2017.08.036

Pool, M., Post, V. E. A., & Simmons, C. T. (2015). Effects of tidal fluctuations and spatial heterogeneity on mixing and spreading in spatially heterogeneous coastal aquifers. *Water Resources Research*, *51*(3), 1570–1585. https://doi.org/10.1002/2014WR016068.Received

Pool, M., Post, V. E. A., & Simmons, C. T. (2014). Effects of tidal fluctuations on mixing and spreading in coastal aquifers: Homogeneous case. *Water Resources Research*, *50*(8), 6910–6926. https://doi.org/10.1002/2014WR015534.Received

Saenger, N., P. K. Kitanidis, and R. L. Street. 2005. A numerical study of surface-subsurface exchange processes at a riffle-pool pair in the Lahn River, Germany. Water Resources Research 41:W12424.

Sawyer, A. H., Cardenas, M. B., Bomar, A., & Mackey, M. (2009). Impact of dam operations on hyporheic exchange in the riparian zone of a regulated river. *Hydrological Processes*, *23*, 2129–2137. https://doi.org/10.1002/hyp7324

Schmadel, N. M., Ward, A. S., Lowry, C. S., & Malzone, J. M. (2016). Hyporheic exchange contolled by dynamic hydrologic boundary conditions. *Geophysical Research Letters*, 1–10. https://doi.org/10.1002/2016GL068286.Received

Sinha, S., Hardy, R. J., Blois, G., Best, J. L., & Smith, G. H. S. (2017). Permeability on Determining Flow Structures Over River Dunes. *Water Resources Research*, *53*(4), 3067–3086. https://doi.org/10.1002/2016WR019662.Received

Spanning, R. J. M., Richardson, D. J., & Ferguson, S. J. (2007). Chapter 1 - Introduction to the Biochemistry and Molecular Biology of Denitrification. In H. Bothe, S. J. Ferguson, & W. E. Newton (Eds.), *Biology of the Nitrogen Cycle* (pp. 3–20). Amsterdam: Elsevier. https://doi.org/https://doi.org/10.1016/B978-044452857-5.50002-3

Squillace, P. J., Thurman, E. M., & Furlong, E. T. (1993). Groundwater As a Nonpoint-Source of Atrazine and Deethylatrazine in a River During Base-Flow Conditions. *Water Resources Research*, *29*(6), 1719–1729.

Squillace, P. J. (1996). Observed and simulated movement of bank-storage water. *Ground Water*, *34*(1), 121–134. https://doi.org/10.1111/j.1745-6584.1996.tb01872.x

Storey, R. G., K. W. F. Howard, and D. D. Williams. 2003. Factors controlling riffle-scale hyporheic exchange flows and their seasonal changes in a gaining stream: A three-dimensional groundwater flow model. Water Resources Research 39:1034.

Tonina, D. and J. M. Buffington. 2011. Effects of stream discharge, alluvial depth and bar amplitude on hyporheic flow in pool-riffle channels. Water Resources Research 47.

Triska, F. J., Kennedy, V. C., Avanzino, R. J., Zellweger, G. W., & Bencala, K. E. (1989). Retention and Transport of Nutrients in a Third-Order Stream in Northwestern California : Hyporheic Processes. *Ecology*, *70*(6), 1893–1905.

W. Harvey, J., & J. Wagner, B. (2000). *Quantifying Hydrologic Interactions Between Streams and Their Subsurface Hyporheic Zones*. *Streams and Ground Waters*. https://doi.org/10.1016/B978-012389845-6/50002-8

White, D. S. (1993). Perspectives on defining and delineating hyporheic zones. *Journal of the North American Benthological Society*, *12*(1), 61–69.

Winter, T. C., Harvey, J. W., Franke, O. L., & Alley, W. M. (1998). Ground water and surface water: A single resource. *USGS Publications*, 79. https://doi.org/10.3389/fpsyg.2012.00044

Zarnetske, J. P., Haggerty, R., Wondzell, S. M., & Baker, M. A. (2011). Dynamics of nitrate production and removal as a function of residence time in the hyporheic zone. *Journal of Geophysical Research: Biogeosciences*, *116*(1), 1–12. https://doi.org/10.1029/2010JG001356

Zarnetske, J. P., R. Haggerty, S. M. Wondzell, and M. A. Baker. (2011). Dynamics of nitrate production and removal as a function of residence time in the hyporheic zone. Journal of Geophysical Research-Biogeosciences 116:G01025.

Zarnetske, J. P., Haggerty, R., Wondzell, S. M., Bokil, V. A., & González-Pinzón, R. (2012). Coupled transport and reaction kinetics control the nitrate source-sink function of hyporheic zones. *Water Resources Research*, *48*(11), 1–15. https://doi.org/10.1029/2012WR011894

Zimmer, M. A., & Lautz, L. K. (2014). Temporal and spatial response of hyporheic zone geochemistry to a storm event. *Hydrological Processes*, *28*(4), 2324–2337. https://doi.org/10.1002/hyp.9778

2. Effect of Surface Water Stage Variation on Mixing-Dependent Hyporheic Denitrification in Riverbed Dunes

In Preparation for Water Resources Research

Lauren Eastes, Erich T. Hester*, and Mark A. Widdowson

Department of Civil and Environmental Engineering, Virginia Tech, Blacksburg, VA 24060

Corresponding Author:
Erich T. Hester
Department of Civil and Environmental Engineering
Virginia Tech
220-D Patton Hall
Blacksburg, VA 24061
Email: ehester@vt.edu
Phone: 540-231-9758

Other Authors:
Lauren A. Eastes
Department of Civil and Environmental Engineering
Virginia Tech
200 Patton Hall
Blacksburg, VA 24061

Mark A. Widdowson
Department of Civil and Environmental Engineering
Virginia Tech
220-A Patton Hall
Blacksburg, VA 24061

ABSTRACT

Increased reactive nitrogen from human activities negatively affects surface water (SW) quality. The hyporheic zone, where SW and groundwater interact, possesses unique biogeochemical conditions that can attenuate contaminants (e.g., denitrification). Mixing-dependent reactions that require components from both water sources may the last chance for groundwater contaminants to react before entering surface water. Previous research explored the effect of heterogeneity on mixing-dependent denitrification in the hyporheic zone but did not address the effects of varying SW depth (e.g., from storms, seasons, tides, dam operation) which has been hypothesized as a control. We simulated steady and unsteady hyporheic flow and transport through a riverbed dune using MODFLOW and SEAM3D, and varied SW depth, degree of sediment heterogeneity, amplitude and frequency of sinusoidal fluctuations, among others. We found that increasing steady state surface water depth from 0.1 to 1.0 m increased non-mixing dependent aerobic respiration by 270% and mixing-dependent denitrification by 78% in homogeneous sediment. Mixing-dependent reactions thus would be stronger when SW stage is elevated during peak floods, high tide, peak dam release, and wintertime. However, the net effect of daily SW oscillations (including variation of amplitude, period, and rate of change) relative to the equivalent average SW depth on mixing dependent denitrification in homogeneous sediment was minimal. Increasing heterogeneity of hydraulic conductivity (i.e. correlation length) increased flow focusing and mixing-dependent denitrification by 20-30%. There is potential for the hyporheic zone to attenuate NO_3^- in upwelling groundwater plumes, but with seasonal variations. Restoration efforts may be able to maximize the potential for mixing-dependent reactions in the hyporheic zone by increasing residence times.

2.1 Introduction

The hyporheic zone is the area of exchange between surface water and groundwater within the sediment of streams, rivers, and estuaries [*Brunke and Gonser*, 1997; *Harvey and Wagner*, 2000, *White*, 1993]. Hyporheic exchange is driven by many hydrologic factors, including flow over riverbed ripples and dunes [*Elliott and Brooks*, 1997a,b; *Packman*, 2004]; larger morphological forms such as cascades, riffles, and meanders [*Cardenas*, 2009a]; and flow obstructions such as logs, boulders, weirs, or dams [*Hester et al.*, 2008; *Winter et al*., 1998]. In particular, dune bedforms are commonly found in medium to large waterways, and the hydraulics of them have been well-studied [*Cardenas and Wilson*, 2007; *Elliott and Brooks*, 1997a,b; *Sinha*, 2017]. In a hyporheic flow cell, a hydraulic gradient drives bidirectional flow through the riverbed, where the surface water enters the subsurface then reenters the surface water flow [*White*, 1993; *Winter et al.*, 1998]. The hyporheic zone exhibits differences in chemical, biological, and hydrologic properties from both surface and groundwater [*Peralta-Maraver*, 2018; *White*, 1993] that allow comparative enhancement of reactions and microbial processes such as denitrification [*Duff and Triska*, 1990; *Hill and Lymburner*, 1998; *Triska et al.*, 1989; *Winter*, 1993; *Zarnetske et al.*, 2011].

2.1.1 Mixing-dependent denitrification in the hyporheic zone

One particularly important hyporheic reaction is denitrification [*Duff and Triska*, 1990; *Gomez-Valez et al.*, 2015; *Hill and Lymburner*, 1998; *Triska et al.*, 1989; *Zarnetske*, 2011] as it removes excess nitrogen, a widespread pollutant in surface water and groundwater [*Dubrovsky et al.*, 2010]. Reactive nitrogen from agricultural runoff and human/livestock sewage [*Braun*, 2007] are converted from NO_3^- to unreactive N_2 in anoxic conditions in the presence of labile dissolved organic carbon (DOC) [*Spanning et al*., 2008].

Recent studies have emphasized the distinction between mixing-dependent and non-mixing dependent reactions in the hyporheic zone [*Hester et al.*, 2014; *Hester et al.*, 2017; *Marzadri et al.*, 2016; *Naranjo*, 2015]. Non-mixing dependent reactions are those where all reactants come from the same source water and intermixing among source waters is not required [*Hester et al.*, 2013]. In the hyporheic zone, this occurs where all reactants come from surface water or all come from groundwater along the same flowpaths. Most prior studies of hyporheic

reactions focus on quantifying non-mixing dependent reactions [*Bardini et al.*, 2012; *Boano et al.*, 2010; *Harvey et al.*, 2013; *Zarnetske*, 2012].

Some reactions occur only if different source waters directly mix. Mixing-dependent reactions in groundwater has primarily been explored in deeper aquifer studies, where contaminant plumes in groundwater are attenuated at the fringe of the plume [*Bauer et al.*, 2009; *Castro-Alcalá et al.*, 2012; *Cirpka et al.*, 1999]. In the hyporheic zone, mixing-dependent reactions require reactants from both surface water and groundwater, and occur at mixing zones between downwelling surface water and upwelling groundwater. Some prior studies have focused on contaminant processes in riverbed sediments where mixing dependent reactions may have occurred but this was not confirmed [*Conant et al.*, 2004; *Kennedy et al.*, 2009; *Landmeyer et al.*, 2010; *Moser et al.*, 2003]. However, very few hyporheic studies have focused on a mixing-dependent reactions [*Hester et al.*, 2013; *Hester et al.*, 2014; *Naranjo*, 2015], yet these represent the last chance for some groundwater contaminants to be degraded before entering more ecologically sensitive surface waters.

Controls on mixing-dependent reactions in the hyporheic zone have received little study. Yet we do know that spatial heterogeneity of hydraulic conductivity can increase such reactions in some cases [*Hester et al.*, 2014], similar to deeper aquifer studies [*Bauer*, 2009]. There has also been speculation that unsteady boundary conditions in possible conjunction with heterogeneity could increase mixing dependent reactions in groundwater [*Neeper*, 2001]. This is particularly relevant in the hyporheic zone with close proximity to surface water fluctuations [*Hester et al.*, 2017]. However, to our knowledge, prior studies have not evaluated the effects of variations in surface water heads on mixing-dependent hyporheic reactions, either in homogeneous or heterogeneous conditions.

2.1.2 Effect of surface water fluctuation

There are many reasons that river stage may fluctuate. Storms are pulse events that can sharply increase river stage for hours [*Hopkinson and Walburn*, 2015] to days [*Dudley-Southern and Binley, 2015; Malzone et al., 2016*]. A rapidly rising river stage can lead to reversal of vertical hydraulic gradients, even generating downwelling conditions in a gaining stream to induce hyporheic exchange [*Dudley-Southern and Binley*, 2015]. Storms can affect stage both in

the river channel and in neighboring groundwater. This can create competing effects of 1) increased surface water entering the bed as channel stage increases thereby enlarging the hyporheic zone and 2) increased hydraulic gradient toward the channel as precipitation recharges the underlying aquifer thereby compressing the hyporheic zone [*Zimmer and Lautz,* 2014].

Many sources of river stage fluctuation, including snowmelt [*Loheide and Lundquist*, 2009], tidal cycles [*Bianchin et al.*, 2011; *Pool et al.*, 2014; *Pool et al.*, 2015], dam operations [*Sawyer et al.*, 2009] and evapotranspiration [*McCallum and Shanafield*, 2016; *Schmadel et al.*, 2016], fluctuate on a diel scale. These fluctuations can alter and even induce hyporheic exchange spanning over three orders of magnitude [*Schmadel et al.*, 2016]. While storms occur as pulse events, diel fluctuations are regular and cyclical in their occurrence. They are often modelled as a sinusoidal curve [*Huang et al.*, 2015; *McCallum and Shanafield*, 2016; *Pool*, 2014; *Pool*, 2015].

Hydropeaking refers to the daily "pulses" of increased river flow often emitted from hydroelectric dams. These lead to large, rapid fluctuations in the water table and a laterally expanded hyporheic zone, as well as flow directions that regularly reverse [*Sawyer et al.*, 2009]. Streams and rivers near coastlines can be affected by tides, with the strength of the perturbation reduced with distance inland [*Huang et al.*, 2015]. Snowmelt also acts on a diel cycle as more melts during the warmer days than the cooler nights. This is seen in both the water table and the river stage [*Loheide and Lundquist*, 2009].

Antecedent conditions such as moisture, geomorphology, geology, and catchment structure also heavily influence the fluctuations seen in the size and depth of the hyporheic zone. As a result, the time of year is also very important for determining groundwater response because the water table fluctuates on a seasonal scale [*Fitts*, 2013]; if the background discharge is high, the hyporheic zone will undergo less expansion in a storm [*Malzone et al.*, 2016].

Hydraulic fluctuations are important for the water quality of rivers. They have been shown to enhance removal of nitrates [*Gu et al.*, 2012], maintain the natural stream chemistry as river water mixes with the regional groundwater [*McCallum et al.*, 2010], enhance heat exchange with groundwater [*Anderson et al.*, 2011], and even prevent solutes from reaching the channel altogether [*Squillace et al.*, 1993; *Squillace*, 1996]. Unsteady models have shown that increasing the amplitude of fluctuations in river stage produces longer hyporheic flow paths and residence

times [*Schmadel et al.*, 2016], although may only slightly increase the below-stream depth of surface water - groundwater mixing zones during storm events [*Dudley-Southern and Binley*, 2015]. Under flooding conditions, the hyporheic zone can detain some amount of in-stream solutes and potentially retard their overall movement [*Lin and Medina*, 2003].

Previous work has evaluated mixing dependent reactions in the hyporheic zone, including the effects of heterogeneity [*Hester et al.*, 2013; *Hester et al.*, 2014]. However, little is known of the effects of surface water fluctuations on these reactions.

2.1.3 Purpose of study

The purpose of this study was to quantify the effect of river fluctuations on hyporheic exchange and an important hyporheic reaction: mixing-dependent denitrification. Such reactions occur at interfacial mixing zones within riverbed sediments between 1) hyporheic flow cells comprised of downwelling surface water and 2) upwelling groundwater surrounding the flow cells. We used numerical modeling to quantify mixing-dependent denitrification beneath riverbed dunes in a gaining river. The objectives of this study were to: 1) quantify the effects of varying surface water depth on mixing-dependent denitrification under steady state conditions, 2) quantify the effects of unsteady (oscillating) surface water depth on mixing-dependent denitrification, and 3) evaluate the effects of heterogeneity of riverbed sediment in this context.

2.2 Methods

2.2.1 Model domain and equations

We developed a numerical model to evaluate the flow, transport, and biogeochemical reactions occurring within the saturated sediment of one in a series of riverbed dunes. Hyporheic flow is driven by variations in the pressure along the dune caused by drag over the bedform and upwelling groundwater. We varied a series of parameters in a sensitivity analysis as described later in this section. We varied parameters one-at-a-time relative to a basecase rather than stochastically because accurately simulating mixing-dependent reactions requires high spatial resolution to avoid numerical dispersion. This dictates long model run times (typically 4-18 hours) [*Hester et al.*, 2013; *Hester et al.*, 2014].

The model domain was a 2D vertical slice of a dune oriented in the downstream direction with a vertical height of 0.138 m, length in the downstream direction of 0.918 m, and thickness

in the cross-stream direction of 0.01 m. The model bottom was set to 0.5 m below the dune bottom (Figure 1). The total 2D area of the model was 0.515 m^2. Each grid cell was 5.0 mm by 5.0 mm with a cross-stream thickness of 10 mm for a total of 20,619 model cells. This grid size was chosen as an intermediate value to the coarse grid (6.3 mm by 6.3 mm) and the fine grid (4 mm by 4 mm) used in *Hester et al.* [2014]. The coarse and fine grids from *Hester et al.* [2014] found nearly identical rates of consumption for DOC, DO, and NO_3^-, indicating that both grids had very similar amounts of numerical dispersion. In order to limit the run time of the model, we used the 5 mm by 5 mm grid as an acceptable grid size.

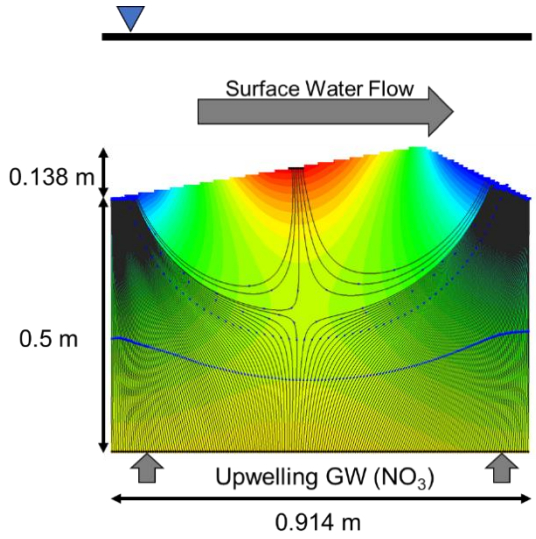

Figure 1: Conceptual figure of the model domain. High piezometric head values are displayed in red and low piezometric head values in blue, with flowlines from surface water moving from high to low piezometric head and flowlines from upwelling groundwater indicating the shape and size of the hyporheic cell.

We used the same groundwater flow, transport, and reaction model as *Hester et al.* [2014]. Both the previous model and ours used MODFLOW and SEAM3D within Groundwater Model Software (GMS). MODFLOW uses a finite-difference approach to solve the three-dimensional groundwater flow equation (Equation 1)

$$\frac{\partial}{\partial x}\left(K_{xx}\frac{\partial h}{\partial x}\right)+\frac{\partial}{\partial y}\left(K_{yy}\frac{\partial h}{\partial y}\right)+\frac{\partial}{\partial z}\left(K_{zz}\frac{\partial h}{\partial z}\right)+W=S_s\frac{\partial h}{\partial t} \qquad \textbf{[1]}$$

where K_{xx}, K_{yy}, and K_{zz} are the hydraulic conductivity along the x, y, and z spatial axes in (LT^{-1}), h is the potentiometric head (L), W is the volumetric flux per unit volume (T^{-1}) that represents sources and sinks of the water, S_s is the specific storage of the media in (L^{-1}), and t is time (T).

SEAM3D is a reactive transport model that was used to simulate advection, dispersion, and Monod biological reactions using the hydraulic output from MODFLOW via

$$\frac{\partial(\theta C^k)}{\partial t} = \frac{\partial}{\partial x_i}\left(\theta D_{ij}\frac{\partial C^k}{\partial x_j}\right) - \frac{\partial}{\partial x_i}(\theta v_i C^k) + W C_s^k + \sum R_k \qquad \textbf{[2]}$$

where θ is porosity of the media, C^k is the dissolved concentration of species k (ML^{-3}), t is time (T), $x_{i,j}$ is the distance on the coordinate axis (L), D_{ij} is the hydrodynamic dispersion coefficient tensor (L^2T^{-1}), v_i is linear pore water velocity (LT^{-1}), C_s^k is the concentration of the source or sink flux for the species k (ML^{-3}) and $\sum R_k$ is the reaction term ($ML^{-3}T^{-1}$). We used SEAM3D to model two Monod biological reactions in addition to advection and dispersion of the dissolved reactants. These reactions were the same as those used in *Hester* [2014]. We used formaldehyde as the dissolved organic carbon (DOC) source for both non-mixing dependent aerobic respiration (Equation 3) within the hyporheic flow cell and mixing-dependent denitrification (Equation 4) between the flow cell and upwelling groundwater.

$$CH_2O + O_2 \rightarrow CO_2 + H_2O \qquad \textbf{[3]}$$

$$5CH_2O + 4NO_3^- + 4H^+ \rightarrow 5CO_2 + 2N_2 + 7H_2O \qquad \textbf{[4]}$$

The reaction term from Equation 2 may be expressed as the following for aerobic respiration and denitrification

$$R_k = \sum_n \left(\frac{M_n}{\theta}\right)(\gamma_{n,k})(v_n)\left(\frac{C_{ED}}{K_{ED}+C_{ED}}\right)\left(\frac{C_{EA}}{K_{EA}+C_{EA}}\right) I \qquad \textbf{[5]}$$

where M_n is the biomass concentration (ML^{-3}) for a given reaction n (for our purposes either aerobic respiration or denitrification), $\gamma_{n,k}$ is the use coefficient for a species k within reaction n, v_n is the maximum specific rate of utilization of substrate for reaction n, C_{ED} is the concentration of the electron donor (DOC) (ML^{-3}), K_{ED} is the half saturation constant of the electron donor (ML^{-3}), C_{EA} is the concentration of the electron acceptor (ML^{-3}), K_{EA} is the half saturation constant of the electron acceptor (ML^{-3}), and I is the inhibition function. The use coefficient

indicates the mass of solute *k* used for each unit mass of the electron donor of reaction *n.* This coefficient would be equal to 1 for calculating the consumption of DOC in either the aerobic respiration or denitrification reaction. The use coefficient of 1.07 for dissolved oxygen (DO) in aerobic respiration and 1.65 for NO_3^- in denitrification are found stoichiometrically. The inhibition function represents the inhibition of denitrification, which is dependent on the DO availability (Equation 6)

$$I = \frac{K_I}{K_I + C_{DO}} \quad \textbf{[6]}$$

where K_I is the inhibition constant for our denitrification reaction (ML^{-3}) and C_{DO} is the DO concentration (ML^{-3}). Aerobic respiration experiences no inhibition, so the inhibition function *I* is equal to 1.

To sum, the consumption of DO via aerobic respiration for our model is

$$R_{DO} = -\left(\frac{M_{AR}}{\theta}\right)(\gamma_{DO,AR})(v_{AR})\left(\frac{C_{DOC}}{K_{DOC}+C_{DOC}}\right)\left(\frac{C_{DO}}{K_{DO}+C_{DO}}\right) \quad \textbf{[7]}$$

The consumption of NO_3^- via denitrification is

$$R_{NO_3^-} = -\left(\frac{M_{DN}}{\theta}\right)(\gamma_{NO_3^-,DN})(v_{DN})\left(\frac{C_{DOC}}{K_{DOC}+C_{DOC}}\right)\left(\frac{C_{NO_3^-}}{K_{NO_3^-}+C_{NO_3^-}}\right)\left(\frac{K_I}{K_I+C_{DO}}\right) \quad \textbf{[8]}$$

And the overall consumption of DOC via both aerobic respiration and denitrification is

$$R_{DOC} = -\left(\frac{M_{AR}}{\theta}\right)(v_{AR})\left(\frac{C_{DOC}}{K_{DOC}+C_{DOC}}\right)\left(\frac{C_{DO}}{K_{DO}+C_{DO}}\right) - \left(\frac{M_{DN}}{\theta}\right)(v_{DN})\left(\frac{C_{DOC}}{K_{DOC}+C_{DOC}}\right)\left(\frac{C_{NO_3^-}}{K_{NO_3^-}+C_{NO_3^-}}\right)\left(\frac{K_I}{K_I+C_{DO}}\right) \quad \textbf{[9]}$$

This approach to modeling nitrate transport with denitrification within the hyporheic environments is consistent with previous studies [*Gu et al.*, 2007; *Hester et al.*, 2014; *Zarnetske et al.*, 2011; *Zarnetske et al.*, 2012]. We did not consider nitrification for this study, which produces NO_3^- from aerobic biotransformation of NH_4^+. Though the balance of nitrification and denitrification does affect the amount of NO_3^- in the system [*Maggi et al.*, 2008], we assume that

NH_4^+ was not present in groundwater or surface water, which enabled investigation of variables controlling mixing- and non-mixing dependent reactions.

2.2.2 Hydraulic model boundary conditions and parameters

2.2.2.1 Boundary conditions

We set the bottom boundary condition as a constant flow boundary of 0.01 m^3/d for all model runs to represent inflowing groundwater. We set the left and right model boundaries (upstream and downstream, respectively) as no flow. For the hydraulic surface water boundary at the top of the model (i.e. the dune surface), we investigated the effect of both a series of steady-state surface water (SW) depths and unsteady SW depth fluctuations.

Changes in steady-state depths represent seasonal flooding conditions where surface water depth changes between seasons but slowly enough that essentially steady-state conditions are sustained over longer time periods. For unsteady fluctuations, we considered both instantaneous changes and sinusoidal changes on typically a daily schedule (Figure 2a). The sinusoidal fluctuation represents varying average SW depth that occurs from diel cycles of processes such as snowmelt, evapotranspiration, and tides. The instantaneous change represents more sudden changes in SW depth that occur due to hydropeaking and certain storm events. For the sinusoidal fluctuations we varied the time period of the fluctuation from 12 to 48 hours (Figure 2b, Table 1,2). We used a 12-hour time period as a minimum to reflect a tidal cycle. We also varied the amplitude of the sinusoidal fluctuation with a 24-hour period (Figure 2c, Table 1,2). All unsteady runs used a 2-day simulation duration, including the 48-hour period. In order to account for this in calculations, the 48-hour run was initialized with the solute concentration fields for the 0.5725 m surface water depth 2-day steady-state run.

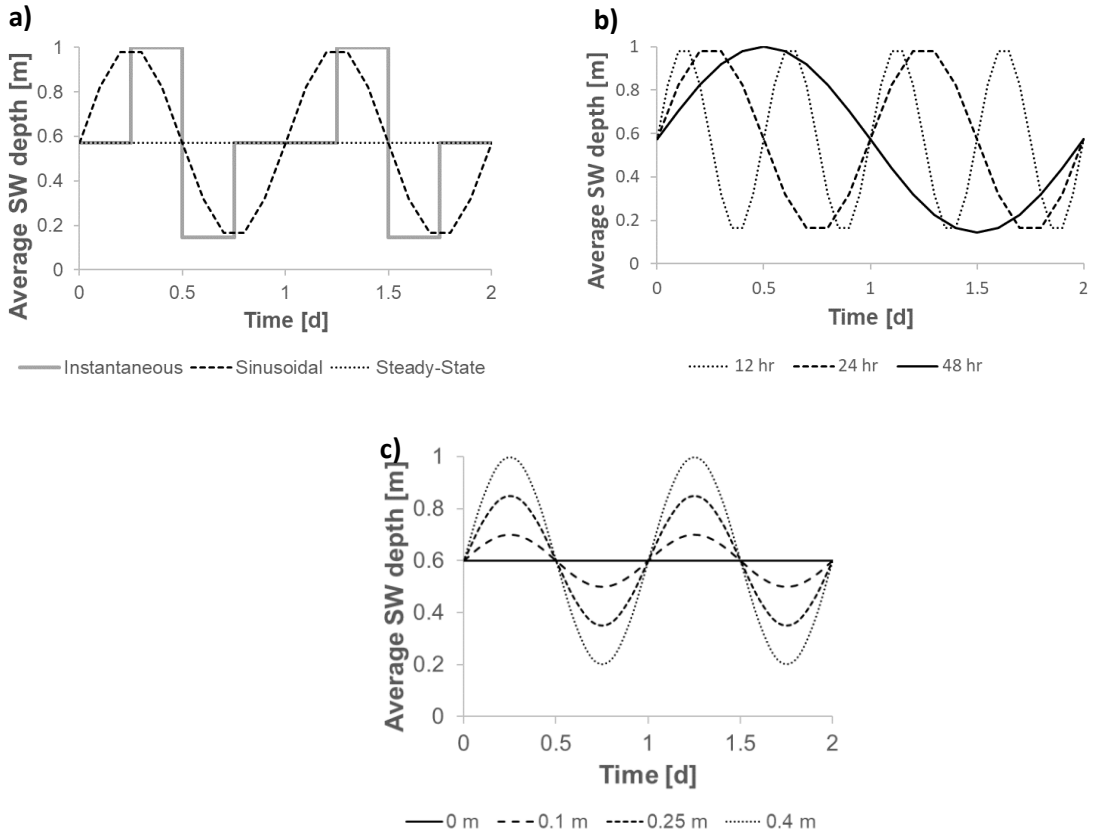

Figure 2: The average surface water (SW) depth over time for a) an instantaneous change in surface water depth and sinusoidally changing surface water depth, b) average surface depth over time for 12-hour, 24-hour, and 48-hour periods of sinusoidal fluctuation, c) average surface water depth across time with varying amplitude of fluctuation

Table 1: Basecase parameters.

Basecase parameters	**Unit**	*Period and Rate of Change Basecase*	*Amplitude Basecase*	*Heterogeneous Basecase*
Surface water boundary condition				
Depth	**m**	0.145-1.0	-	-
Time-averaged depth (d_{avg})	**m**	0.5725	0.6	-
Amplitude	**m**	0.4275	-	-
Period	**hr**	24	24	-
Rate of change	-	sinusoidal	sinusoidal	-
Heterogeneous hydraulic conductivity				
Variance	-	0	0	1.0
Horizontal Correlation Length	**cm**	-	-	4.0

Table 2: Sensitivity analysis parameters and ranges.

		Sensitivity parameter varied					
		Surface water boundary condition				*Heterogeneous hydraulic conductivity*	
	Unit	Depth	Amplitude	Period	Rate of change	Variance	Horizontal correlation length
Surface water boundary condition							
Depth	**m**	0.1-1.0	Fig. 2c	Fig. 2b	Fig. 2a	Fig. 4b	Fig. 4b
Time-averaged depth (d_{avg})	**m**	-	0.6	0.5725	0.5725	-	-
Amplitude	**m**	-	0-0.4	0.4275	0.4275	-	-
Period	**hr**	-	24	12-48	24	-	-
Rate of change	**-**	-	sinusoidal	sinusoidal	instantaneous vs sinusoidal	-	-
Heterogeneous hydraulic conductivity							
Variance	**-**	Fig. 4b	-	-	-	0-1.0	1.0
Horizontal Correlation Length	**cm**	Fig. 4b	-	-	-	4	0.91-9

We determined the upper boundary pressure distribution in all cases except the instantaneous change using

$$d = A * \sin\left(\frac{2\pi}{P} * t\right) + d_{avg} \quad \textbf{[10]}$$

where d is the time-dependent mean flow depth of the surface water defined as depth above the bedform crest plus half of the bedform height (L) [*Fehlman*, 1985], A is the amplitude of the fluctuation (L), P is the period of the fluctuation (T), t is time (T), and d_{avg} is the average depth of the surface water across time (L). For steady-state surface water conditions, the amplitude of the fluctuation is equal to zero, and the time-dependent average depth d is equal to the average depth across time d_{avg}.

We used Manning's equation to estimate the depth-averaged surface water velocity at each depth condition, assuming the river is hydraulically wide (i.e. insignificant cross-stream variation)

$$U = \frac{1}{n} * d^{2/3} S^{1/2} \quad \textbf{[11]}$$

where U is the surface water velocity, S is the slope, and n is Manning's coefficient. Data from Run 12 of *Fehlman* [1985] were used for the slope of the riverbed and Manning's coefficient. We chose this run because most Fehlman experimental water column depths are quite shallow and Run 12 is one of the deeper runs [*Hester*, 2013; *Hester*, 2014]. This run also has the highest surface water velocity and discharge, providing the most form drag. For our simulation, as the river stage was changed, we held slope constant.

We determined the spatial distribution of surface water pressure across the dune using the empirically derived relationship from *Fehlman* [1985]. This was based on a compilation of the pressure data taken by *Fehlman* [1985] over a dune of the same dimensions as the one used for this model and data from studies by *Raudkivi* [1963], *Vanoni and Hwang* [1967], and *Rifai and Smith* [1967] that had been integrated by *Wang* [1983] as well as data from *Vittal et al.* [1977]. *Fehlman* [1985] derived the following expression for the half amplitude of the variation in $h_{dynamic}$, generated by form drag over the dune series:

$$h_m = 0.28\frac{U^2}{2g}\begin{cases}\left(\frac{H/d}{0.34}\right)^{3/8} & H/d \le 0.34\\ \left(\frac{H/d}{0.34}\right)^{3/2} & H/d \ge 0.34\end{cases} \quad \textbf{[12]}$$

where h_m is half of the amplitude of the variation in dynamic head at the bed surface ($h_{dynamic}$) and H is the height of the dune in meters. The coefficient H/d is the relative roughness of the channel. This relationship was developed using conditions with Froude numbers from 0.1 to 0.5 and for relative roughness H/d coefficients from 0.1 to 0.7 [*Fehlman,* 1985]. The Froude number for our system ranged from 0.3 to 0.4, while our H/d ranged from 0.13 to 0.95. This approach has been used for similar applications in *Gomez-Velez et al.* [2015], *Käser et al.* [2013], *Malzone et al.* [2016], *Stonedahl et al.* [2013]. The spatial distribution of heads across the dune, normalized by h_m, is shown in Figure 3 developed by *Elliott and Brooks* [1997]. We then multiplied these normalized values by h_m as determined by Equation 3 for each time step, producing a series of values for $h_{dynamic}$ (Equation 13, Figure 4a).

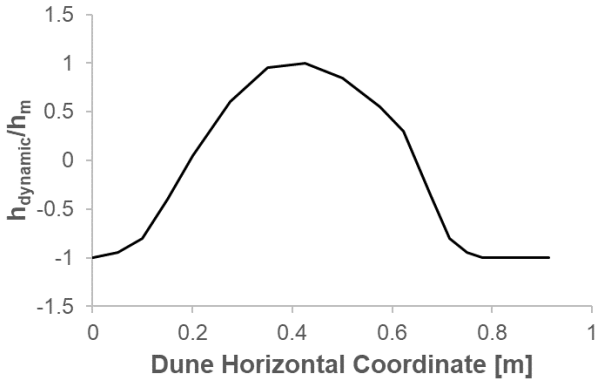

Figure 3: The head distribution along the dune, normalized to the half amplitude, h_m.

We determined the actual surface water head $h_{surface}$ by adding the $h_{dynamic}$ to the static head at each timestep, the latter being equal to time-dependent surface water depth d (Equation 6, Figure 4b).

$$h_{dynamic} = \frac{h_{dynamic}}{h_m} * h_m \quad \textbf{[13]}$$

$$h_{surface} = h_{dynamic} + d \quad \textbf{[14]}$$

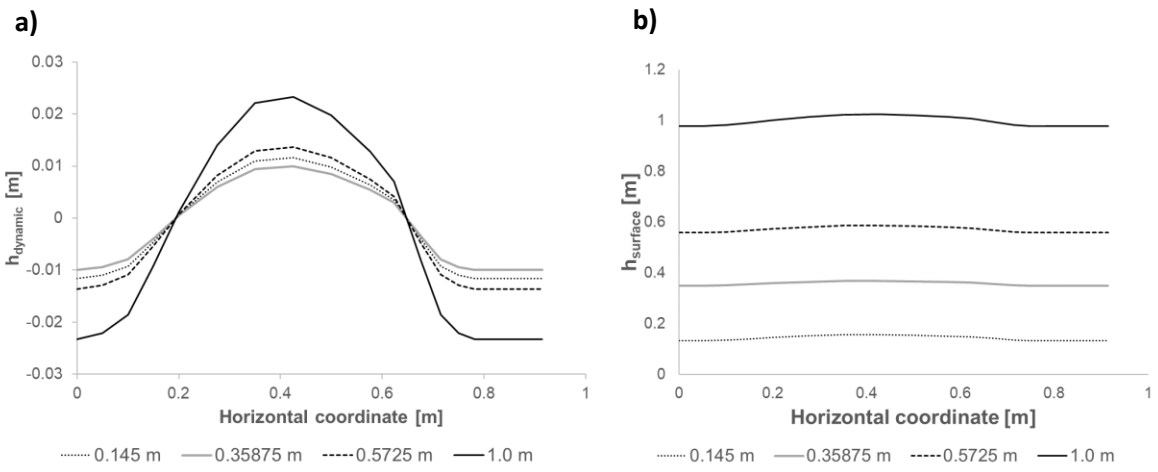

Figure 4: Distributions of the a) dynamic head ($h_{dynamic}$) and b) actual (total) surface water head ($h_{surface}$) for the dune at each horizontal coordinate for a series of time-dependent river depths (d).

2.2.2.2 Groundwater flow parameters

We set hydraulic conductivity uniformly to 25 m/d for all model runs with homogeneous sediment, including those evaluating response to steady-state surface water conditions and those evaluating unsteady surface water conditions. We chose this condition to keep the hyporheic cell within the model dimensions thus avoiding model artifacts associated with flow interaction with model boundaries.

The hydraulic conductivity fields used for model runs with heterogeneous fields were lognormally spatially correlated random fields previously generated in *Hester et al*. [2013]. The heterogeneous basecase used a hydraulic conductivity field with a horizontal correlation length of 4 cm and a variance of 1.0. We then varied the variance and correlation length of heterogeneous fields (Table 1). In order to directly compare heterogeneous model results to those from a homogeneous case, we also ran a model with an equivalent homogeneous hydraulic conductivity of 84.4 m/d, equal to the mean of lnK for the heterogeneous basecase.

To approximate the travel time of particles through the mixing zone, we used 45 tracer particles in MODPATH that started 20 cells (10 cm) below the stagnation point of the upwelling groundwater. This stagnation point occurs at the deepest part of the flow cell and was determined by visually approximating the location at which the upwelling groundwater particles split their flow to either side of the flow cell (Figure 1).

Finally, when investigating the effect of combining both unsteady surface water conditions with heterogeneous sediment, we used the shortest (12-hour) fluctuation period and the longest (9 cm) correlation length. We chose this combination because mixing theoretically should be greatest when the residence time of solute in low hydraulic conductivity zones is similar to the period of fluctuation [*Hester et al.*, 2017; *Neeper*, 2001]. Even our longest correlation length produced residence times shorted than 12 hours, hence we picked the shortest period and longest correlation length to maximize mixing dependent reactions.

2.2.3 Solute transport boundary conditions and parameters

Because we are interested here in hydraulic controls on reactions, we chose SEAM3D surface and groundwater biogeochemical boundary conditions to ensure that the reaction was transport limited, i.e. denitrification primarily occurred within the mixing zone between the hyporheic cell and upwelling groundwater (Table 3). The surface water had relatively high concentrations of DOC and DO, while NO_3^- was only present in the groundwater, similar to basecase 3 of *Hester et al.* [2014]. This is representative of a scenario where groundwater is contaminated by septic systems or agricultural activities, as these plumes typically have high NO_3^- and low DO and DOC, where DO and DOC were consumed in nitrification reactions. While the complete exclusion of NO_3^- from surface water and DOC from groundwater may not be fully realistic, choosing these parameter values ensures that all denitrification occurring in the system is mixing-dependent, allowing it to also represent a wide range of other potential mixing dependent reactions. For example, DO from surface water could mix and react with petroleum hydrocarbons from an upwelling groundwater plume as may be occurring in some of the sites presented in [*Landmeyer et al.* 2010]. .

Table 3: Biogeochemical boundary conditions.

Parameter	Unit	Concentration
Surface water		
DOC	mg/L	50
DO	mg/L	5
NO_3^-	mg/L	0.01
Groundwater		
DOC	mg/L	0
DO	mg/L	0.01
NO_3^-	mg/L	24.8

2.3 Results

2.3.1 Response to steady-state surface water depth

2.3.1.1 Homogeneous sediment

As average surface water depth increased, the mass of DO consumed by non-mixing dependent aerobic respiration within the dune-induced hyporheic flow cell decreased but then increased at the depth of 0.35875 m by 270% (Figure 5a). The trend for percent oxygen consumed was opposite that for mass consumed, because as the mass consumed increased, the percentage of the oxygen entering the dune that underwent aerobic respiration decreased. This indicates that, while increasing the average depth at depths deeper than the inflection point may increase the mass of oxygen consumed, this effect is exceeded by the amount of oxygen that passes through the dune unconsumed. The larger surface water head gradient drives more water into the hyporheic zone, pushing more oxygen back to the surface unreacted.

Results for the mass nitrate consumed by mixing-dependent denitrification showed a similar trend to that of oxygen, increasing with surface water depth by 78% (compare Figure 5a and 5b). However, unlike for oxygen, the trend in the percentage consumed closely mirrored that of the mass undergoing denitrification because nitrate was sourced from a constant-flow boundary of upwelling groundwater. The consumption of dissolved organic carbon (DOC) for both aerobic respiration and denitrification exhibits a similar trend to the DO consumption and denitrification mass responses (Figure 5c).

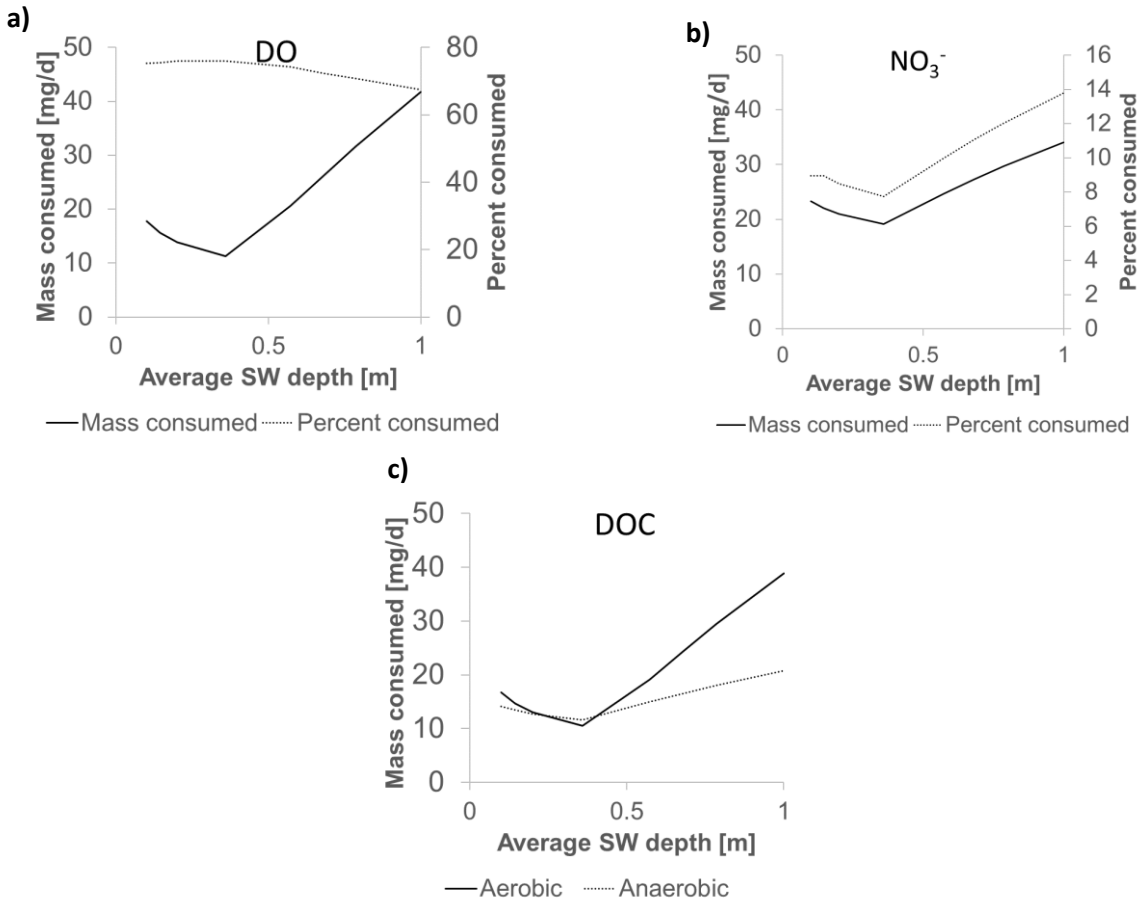

Figure 5: Consumption of a) DO via non-mixing dependent aerobic respiration, b) NO_3^- via mixing-dependent denitrification, and c) DOC via both reactions over a range of average surface water depths from 0.1 m to 1 m. DO=dissolved oxygen, DOC=dissolved organic carbon, SW=surface water. Average SW depth refers to the average depth of the water column in the overlying river.

2.3.1.2 Heterogeneous sediment

2.3.1.2.1 Heterogeneous basecase

We varied average surface water depth for both the basecase heterogeneous K field and the equivalent homogeneous K field. This is to provide a comparison and determine the direct effect of introducing heterogeneity to the system. Both the amount of DO and the percent of incoming DO undergoing non-mixing dependent aerobic respiration were lower for the heterogeneous case relative to the equivalent homogeneous case (Figure 6a) while the amount of mixing-dependent denitrification was similar for both scenarios (Figure 6b).

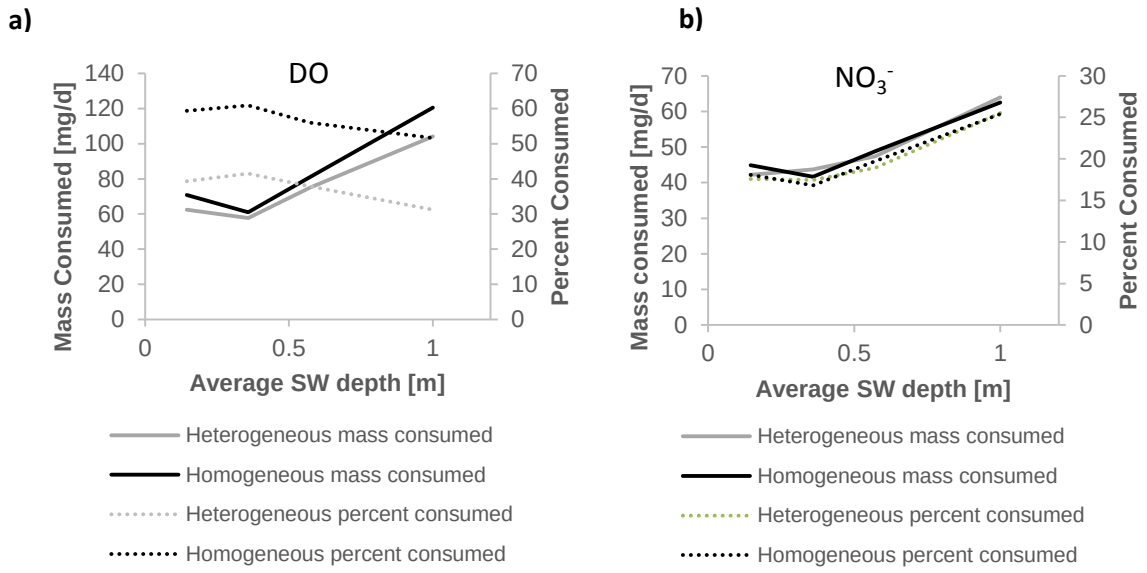

Figure 6: Comparison of a) non-mixing dependent aerobic respiration and b) mixing-dependent denitrification in the heterogeneous and homogeneous basecases. Average surface SW depth refers to time-dependent *d*, which for the steady-state is not changing over time. DO=dissolved oxygen, SW=surface water. The equivalent homogeneous basecase has a hydraulic conductivity field of 84.4 m/d, the log-normal average of the heterogeneous basecase. Note that the homogeneous K used in Figure 5 is 25 m/d, which is different from the equivalent K used here because the heterogeneous fields use have a lognormal mean of 84.4 m/d. This is why the mass consumed in Figures 6ab is larger than that consumed in Figures 5ab.

2.3.1.2.2 Horizontal Correlation Length

For non-mixing dependent aerobic respiration, increasing the correlation length led to a lower percentage of the DO coming in undergoing reaction by ~6% for the heterogeneous case, although similar amounts of mass were consumed (Figure 7a,b). This indicates that the primary effect of altering the correlation length on the aerobic reaction was to increase the total amount of DO entering the system (Figure 7c). This trend did not change much with surface water depth. For mixing-dependent denitrification, increasing the correlation length led to an increase in both mass consumed and percent consumed (Figure 8). This trend was not monotonic, and followed a pattern similar to that in Figure 6 of Hester et al. [2013], indicating the cause of the trend is likely variation in mixing with correlation length. While the mass consumed of NO_3^- increased by about 20-30%, depending on the surface depth, the percent of NO_3^- consumed only exhibited a net increase of ~4.7%. This trend also did not change much with surface water depth.

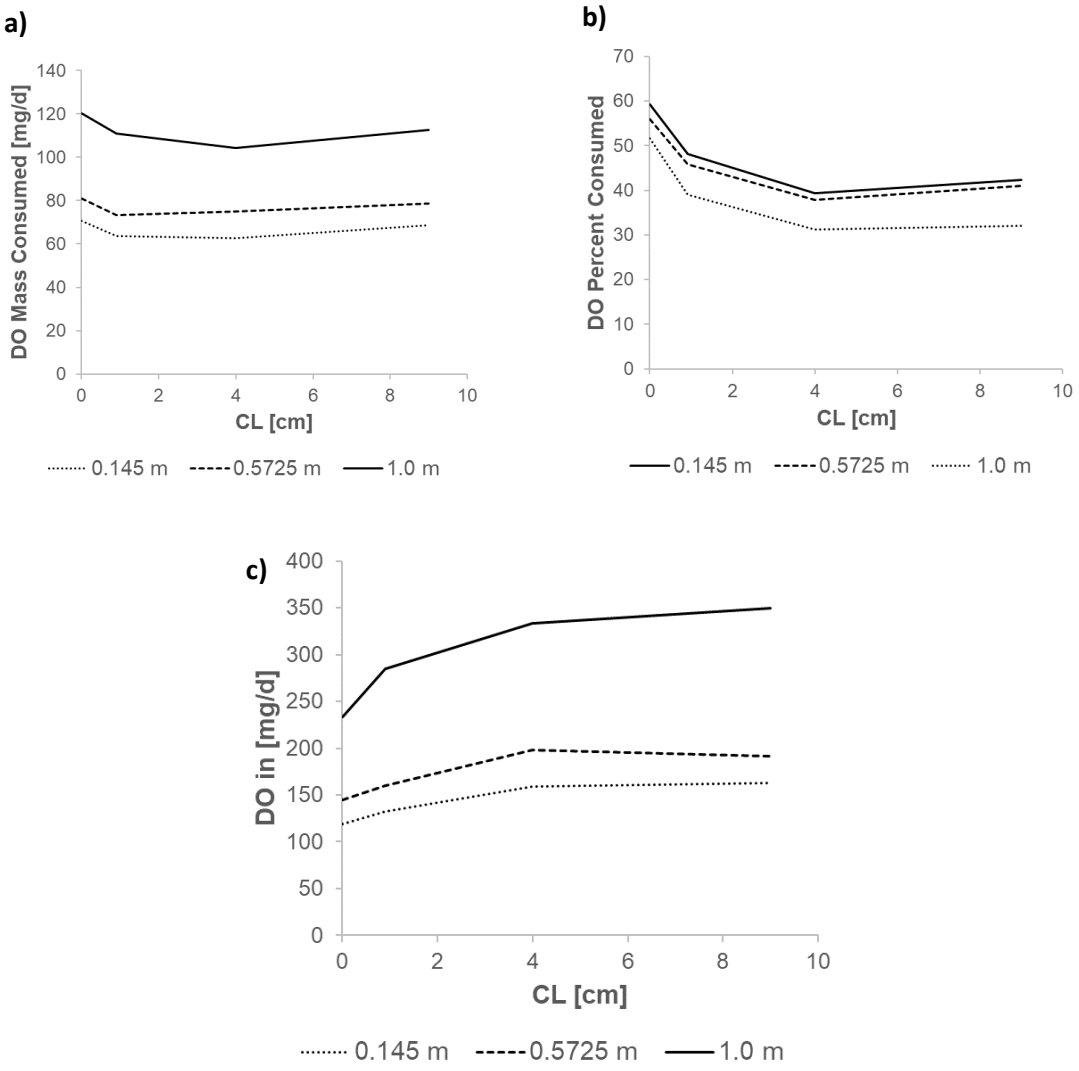

Figure 7: Comparison of non-mixing dependent aerobic respiration by a) mass of oxygen consumed and b) percent of incoming oxygen consumed and c) the rate of DO entering the dune from SW for a range of horizontal correlation lengths. These are steady-state runs with varying average surface water depths. CL=heterogeneous hydraulic conductivity field horizontal correlation length, DO=dissolved oxygen, SW=surface water. The homogeneous case is included as a CL of zero.

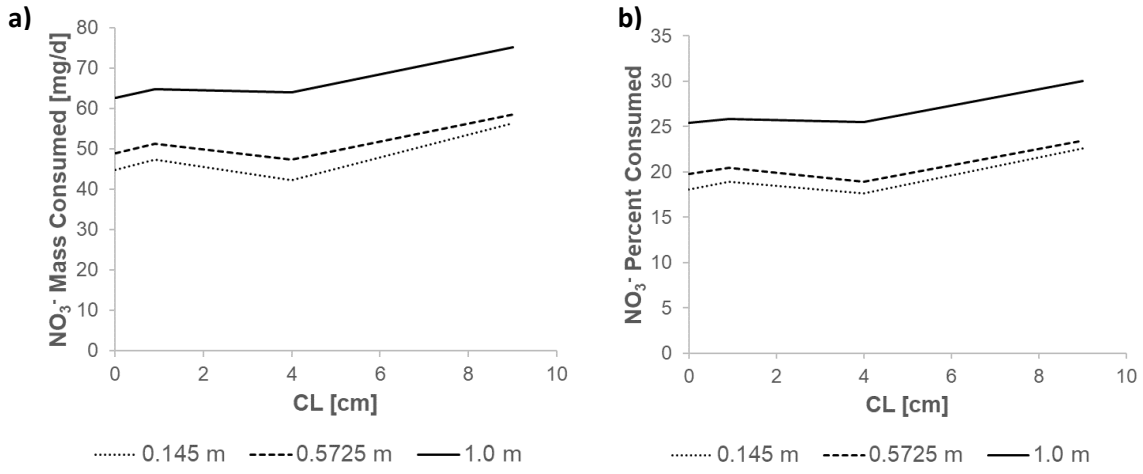

Figure 8: Comparison of mixing-dependent denitrification by a) mass consumed and b) percent of incoming nitrate undergoing reaction for a range of horizontal correlation lengths. These are steady-state runs with varying average surface water depths. CL= heterogeneous hydraulic conductivity field horizontal correlation length, SW=surface water. The homogeneous case is included as a CL of zero.

2.3.1.2.3 Variance

The effect of the variance of the heterogeneous fields was stronger in non-mixing dependent aerobic respiration than mixing-dependent denitrification. As the variance increased, less DO underwent reaction (Figure 9a) and a lower overall percentage of the DO entering the system was consumed (Figure 9b). The response of the percentage of DO consumed (~20% for each surface water depth) was more pronounced than that of the overall amount of DO consumed; this is due to the increased amount of DO entering the system for the higher variance heterogeneous fields (Figure 9c). This decrease in both the amount and percent of DO consumed is similar to the trends seen previously *Hester et al.* [2014]. This effect did not change much with surface water depth, but for all variables in Figure 9 the difference in mass of DO entering the model and consumed between the homogeneous and heterogeneous cases peaked at the greatest surface water depth. This again may reflect higher surface water heads driving more oxygen into the sediment under transport limited conditions. The response of mixing-dependent denitrification to changes in variance is less clear (Figure 10) with an overall variation in mass consumed of NO_3^- of about 4% and variation in percent of NO_3^- consumed of ~0.5%, again

consistent with *Hester et al.* [2014]. This effect did not vary in any obvious way with surface water depth.

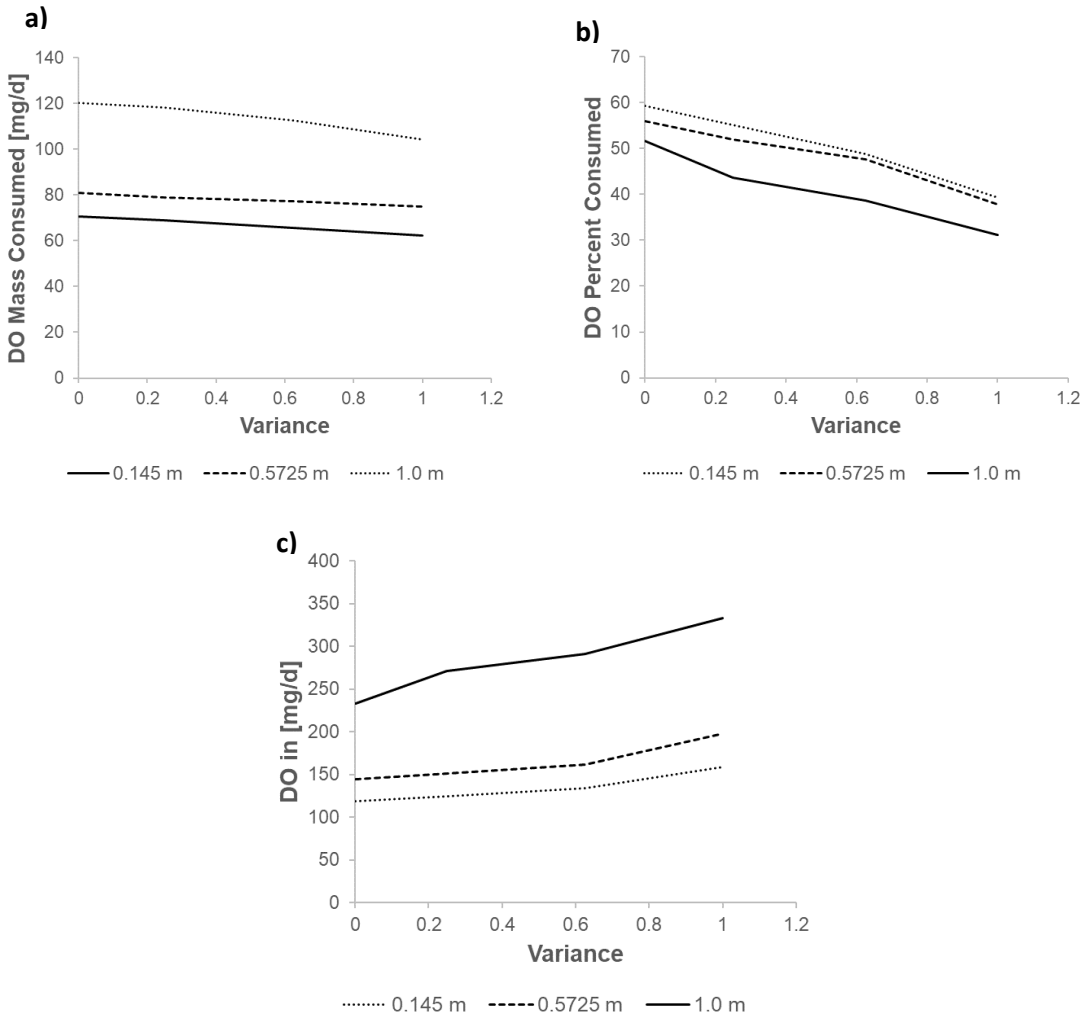

Figure 9: Comparison of a, b) non-mixing dependent aerobic respiration c) DO entering the dune from SW for a range of variances in heterogeneity. DO=dissolved oxygen, SW=surface water. These are steady-state runs with varying average surface water depths.

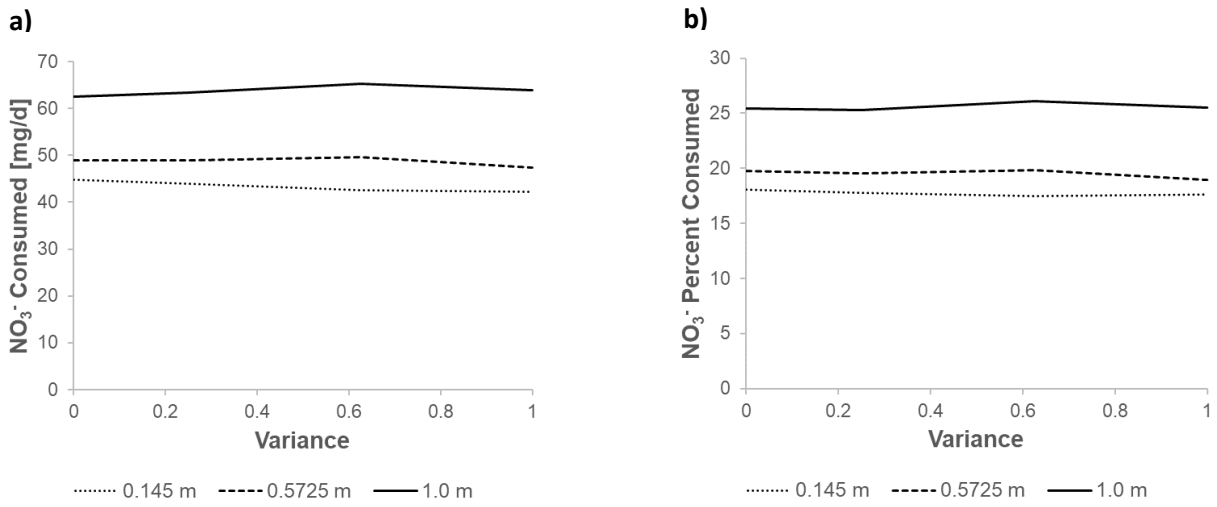

Figure 10: Comparison of mixing-dependent denitrification by a) mass consumed and b) percent of incoming nitrate undergoing reaction for a range of variances in heterogeneity. DO=dissolved oxygen, SW=surface water. These are steady-state runs on with varying average surface water depths.

2.3.2 Response to unsteady surface water depth

2.3.2.1 Homogeneous sediment

2.3.2.1.1 Amplitude of fluctuation

The response in the consumption of DOC and DO by non-mixing dependent aerobic respiration, and DOC and nitrate by mixing-dependent denitrification, to the changes in amplitude of surface water fluctuation was low (Figure 11). This indicates that daily fluctuation amplitude affects how far mixing zones move back and forth in the sediment, but this change in movement in turn does not much affect the net time-averaged effect of both non-mixing dependent and mixing-dependent reactions.

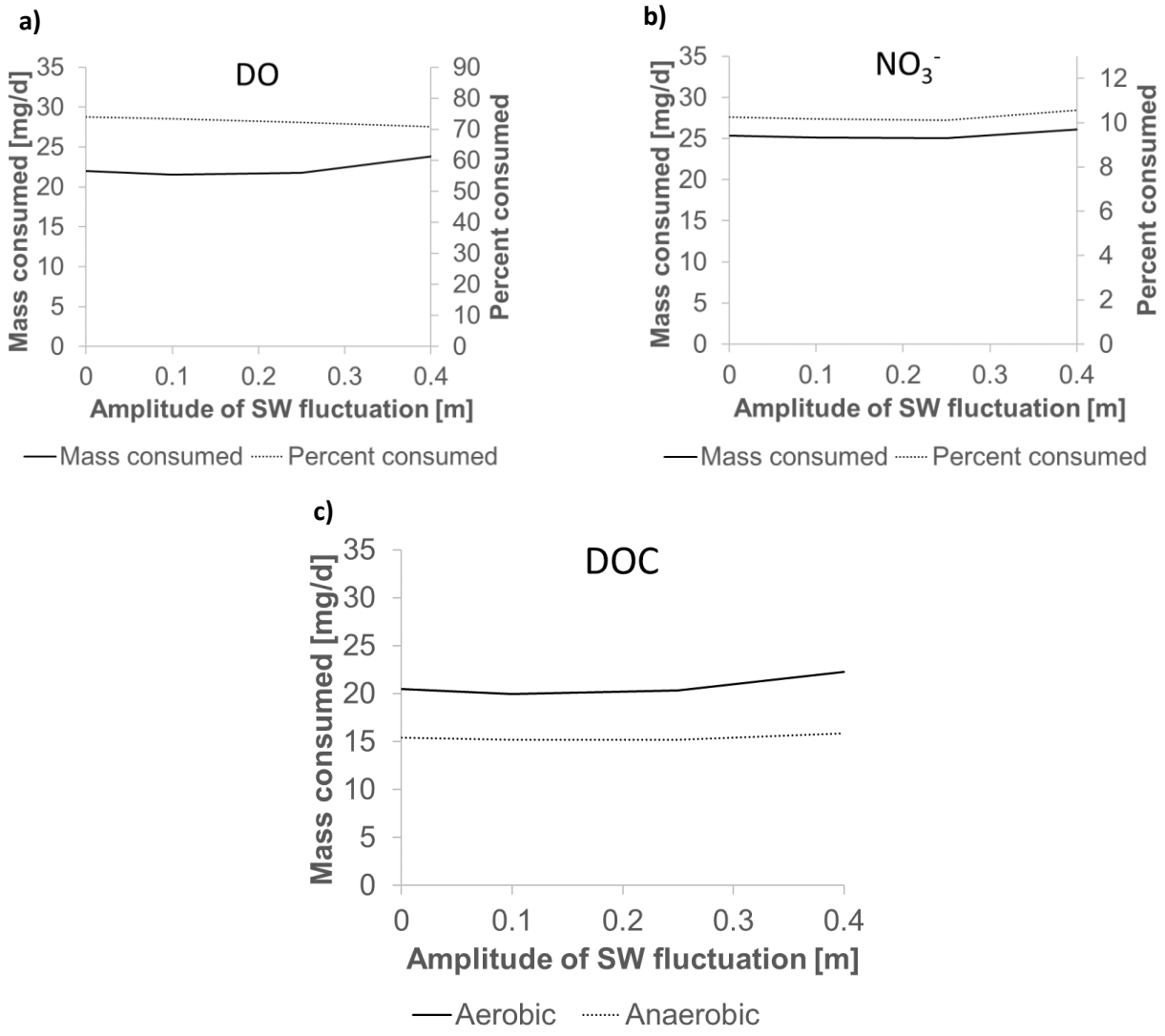

Figure 11: Consumption of a) DO by non-mixing dependent aerobic respiration, b) NO_3^- by mixing-dependent denitrification, and c) DOC by both reactions over a range of amplitudes of surface water depth fluctuation in a homogeneous dune. DO=dissolved oxygen, DOC=dissolved organic carbon, SW=surface water. Model run time was two days, values reported are for the second day to allow for system adjustment for contaminant transport.

2.3.2.1.2 Period of fluctuation

Mixing-dependent denitrification decreased slightly with increasing fluctuation period, perhaps indicating that less frequent fluctuations give rise to less mixing and hence less mixing-dependent reactions.

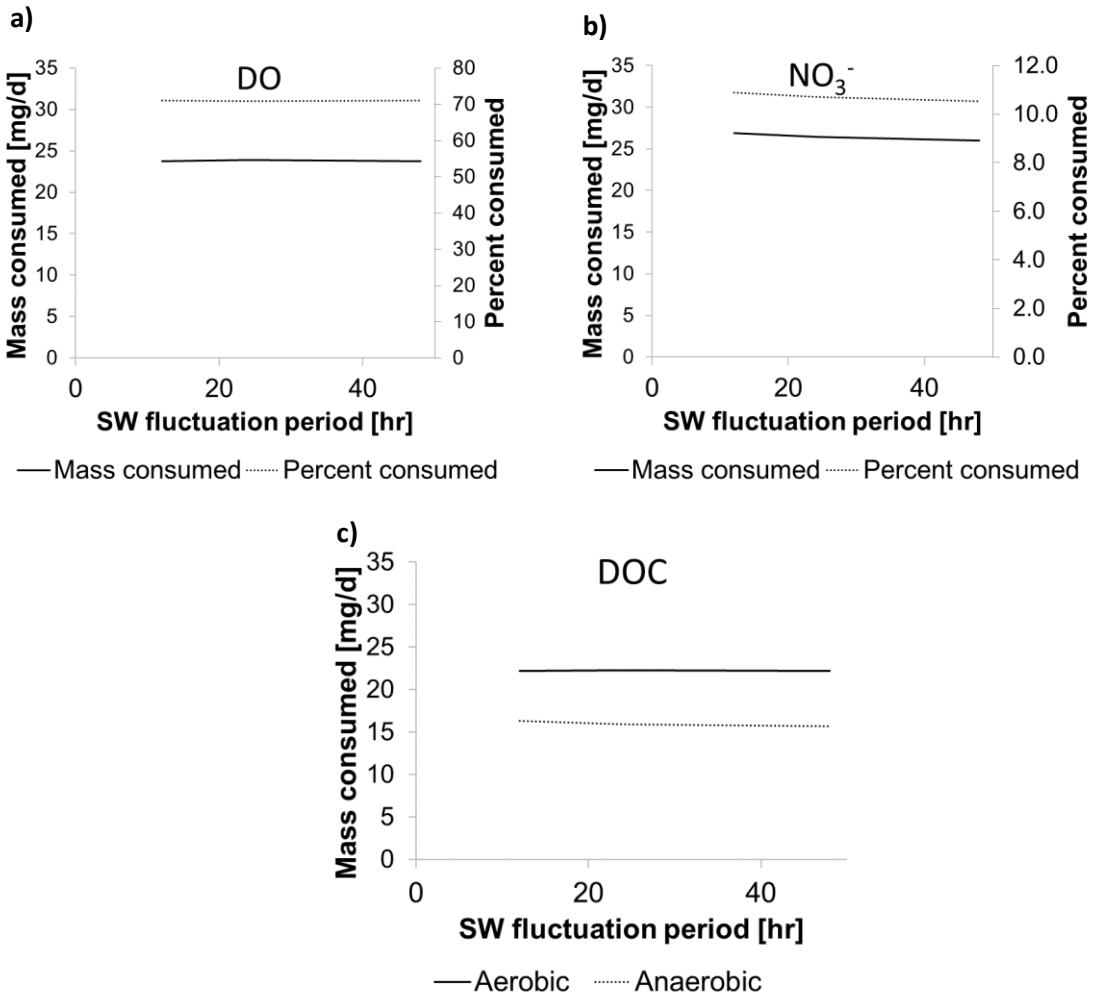

Figure 12: Consumption of a) DO via non-mixing dependent aerobic respiration, b) NO_3^- via mixing-dependent denitrification, and c) DOC via both reactions over a range of periods of fluctuations from 12 to 48 hours for a homogeneous dune. DO=dissolved oxygen, DOC= dissolved organic carbon, SW=surface water. Model run time was two days, values reported are for the second day to allow for system adjustment for contaminant transport, with the exception of the 48-hour period which was averaged over the full two days. To account for this, the 48-hour period was initialized with the contaminant concentration conditions of the steady-state run for 0.5725 m. This is the $h_{surface}$ condition at t=0 of the 48-hour run.

Although the long-term net effect of varying SW fluctuation period on reactions was minor (Figure 12), the effect on temporal dynamics was significant in certain cases. The response in DOC consumption over time for the different fluctuation period durations was more apparent for the aerobic non-mixing dependent reaction than for anaerobic denitrification (Figure 13). The aerobic reaction saw large fluctuations coinciding with the changes in the average surface water depth (Figure 13), while there was significantly less variation in denitrification. In particular, the

solid lines represent non-mixing dependent aerobic respiration and deviated from each other a maximum of ~10 g while the dotted lines representing mixing-dependent denitrification deviated from each other a maximum of ~2.5 g (Figure 13).

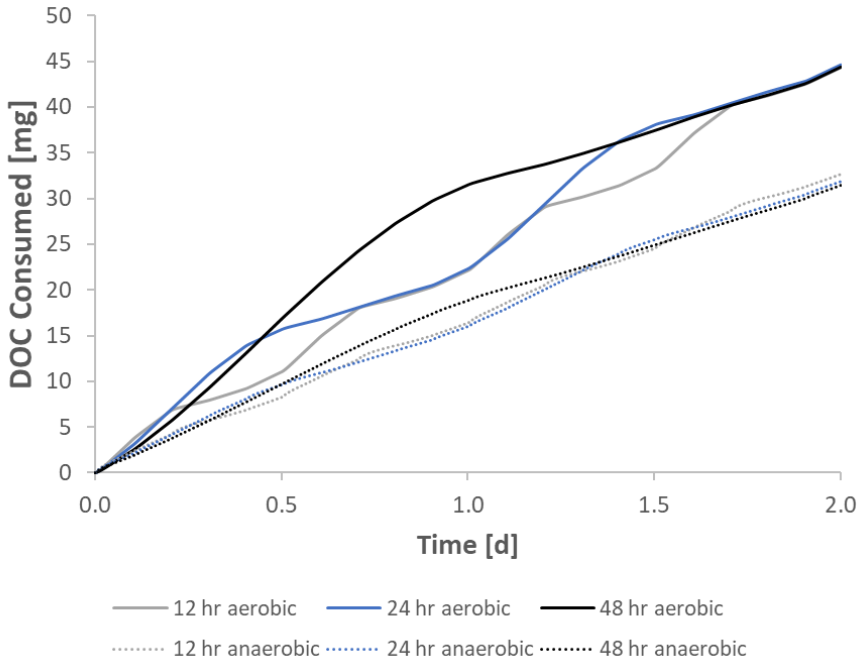

Figure 13: DOC consumption from the aerobic non-mixing dependent reaction and anaerobic mixing dependent reaction (denitrification) over time for the varying periods of sinusoidal surface water fluctuation in a homogeneous dune. DOC=dissolved organic carbon. We plotted DOC consumption in particular because it is a surrogate for the reactions of interest in this study. Specifically, aerobic DOC consumption over time is proportionally related to the DO consumed by a factor equal to the use coefficient while the anaerobic DOC consumption is proportional to the NO_3^- consumed. Looking at the mass consumption of DOC therefore provides a direct comparison of trends in the aerobic respiration and denitrification reactions.

2.3.2.1.3 Rate of change

The instantaneous change in surface water depth generated slightly greater rates of both non-mixing dependent aerobic respiration and mixing dependent denitrification in comparison to the gradual sinusoidal shape. In particular, the percent DO consumed by aerobic respiration increased by ~1.5% and the percent of NO_3^- consumed increased by only 0.2% (Table 4).

Varying the rate of the SW depth fluctuations affected the temporal dynamics of DOC consumption by non-mixing dependent aerobic respiration more that it affected the temporal

dynamics of DOC consumed by mixing-dependent denitrification (Figure 14). In particular, the mass of DOC consumed via aerobic respiration with the sinusoidal surface water fluctuation deviated from that consumed by an instantaneous change by a maximum of ~4.1 mg, while the maximum deviation of DOC consumed via denitrification was ~1.1 mg.

Table 4: Comparison of the non-mixing dependent aerobic respiration and mixing-dependent denitrification occurring during the instantaneous surface water depth change and the sinusoidal fluctuation. A steady-state run at the average surface water depth over time was used for comparison. The model run time was two days, and the values reported are for the second day to allow for the contaminant transport to undergo system adjustment.

	DOC Biodegraded			**O2 Biodegraded**		**NO_3^- Biodegraded**	
	aerobic [mg/d]	anaerobic [mg/d]	Total [mg/d]	Mass [mg/d]	Percent consumed [%]	Mass [mg/d]	Percent consumed [%]
Instantaneous	22.9	16.4	39.2	24.5	71.4	27.0	10.9
Sinusoidal	22.3	15.9	38.3	23.9	70.8	26.5	10.7
Steady-State	19.2	14.9	34.1	20.6	74.2	24.6	10.0

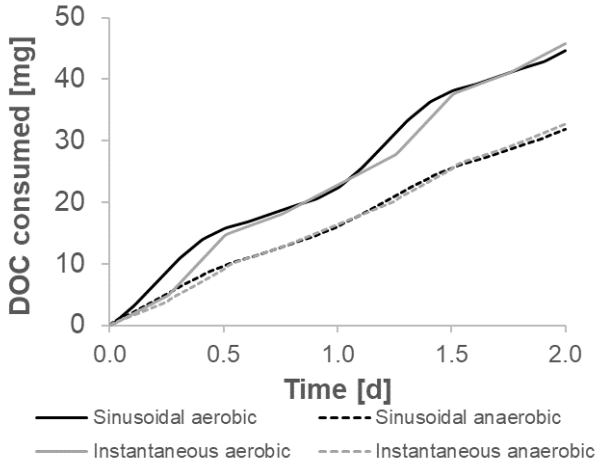

Figure 14: DOC consumption over time for the "hat" and sinusoidal surface water fluctuations over time. DOC=dissolved organic carbon.

2.3.2.2 Heterogeneous sediment

The effect of transient hydraulic head on oxygen and nitrate consumption in the heterogeneous fields was similar to that on the homogeneous fields: aerobic respiration and denitrification only minimally elevated from the corresponding steady-state run of the time-

averaged depth (Table 5). Aerobic respiration increased from 76.8 mg/d to 82.2 mg/d of DO consumed, and denitrification increased from 58.4 mg/d to 62.6 mg/d.

Table 5: DO consumption through non-mixing dependent aerobic respiration and NO3- consumption through mixing-dependent denitrification for a 12-hour period sinusoidal fluctuation between 0.145 m and 1.0 m surface water depth and steady-state runs at the minimum SW depth, time-averaged SW depth, and maximum SW depth.

Runs	Total mass in [mg/d]		Rate of consumption [mg/d]		Percent consumed	
	DO	NO_3^-	DO	NO_3^-	DO	NO_3^-
12 hr sine	218.9	248.9	82.2	62.6	37.6	25.2
Steady 0.145 m	159.8	248.8	67.8	56.2	42.5	22.6
Steady 0.5725 m	190.9	249.4	76.8	58.4	40.2	23.4
Steady 1.0 m	345.3	250.2	112.1	75.2	32.5	30.1

2.4 Discussion

2.4.1 Physical controls on riverbed mixing and reactions

In our steady state results, representative of seasonal variation in surface water depth, all trends between reactant consumption and SW depth (e.g., Figures 5-6) exhibit an inflection point around an average depth of 0.40 m. This is due to the empirically derived equations used to specify the pressure distribution across the dune surface (Figure 4), which inflect at a depth where relative roughness, *H/d*, is equal to 0.34 [*Elliott and Brooks*, 1997]. At the inflection point, the gradient in the $h_{dynamic}$ with respect to surface water depth reaches zero. In other words, the range in the $h_{dynamic}$ decreases as surface water depth increases until the inflection point, then the range begins to increase again. The trend for d > 0.4 m makes intuitive sense in that increasing flow depth implies increasing velocity, and hence form drag from current over the dunes [*Cardenas and Wilson*, 2006; *Cardenas and Wilson*, 2007]. The empirical equations we used are originally from *Fehlman* [1985], but neither *Fehlman* [1985] nor *Elliott and Brooks* [1997] give a mechanistic explanation for why the trend is different for *H/d* less than 0.34. For these reasons, and because d > 0.4 is the largest portion of our x-axis, we focus on that portion of the depth range.

The overall increase in mixing-dependent reaction of about 78% for NO_3^- consumed occurring at surface water depths greater than the inflection point (e.g., Figure 5) is likely related to increased mixing zone size (Figure 15). As the pressure differential across the dune increased, the surface water penetrated the dune more deeply which caused the length and hence volume of the mixing zone to increase by a normalized value of 0.016 (Figure 16). This indicates that these mixing-dependent reactions are transport limited. Aerobic respiration also increased due to the increase in size of the hyporheic flow cell. The effect of increasing surface water depth in this study is analogous to decreasing upwelling groundwater flow in *Hester et al.* [2014]. Both changes increased both the amount of mass reacted and the percentage consumed by increasing the hyporheic flow cell size. Any longer-term trends in surface water depth, i.e. operating on a timescale of weeks to months, could produce significant variation in denitrification rates. This is indicative of possible seasonal variations in rates of denitrification within river systems.

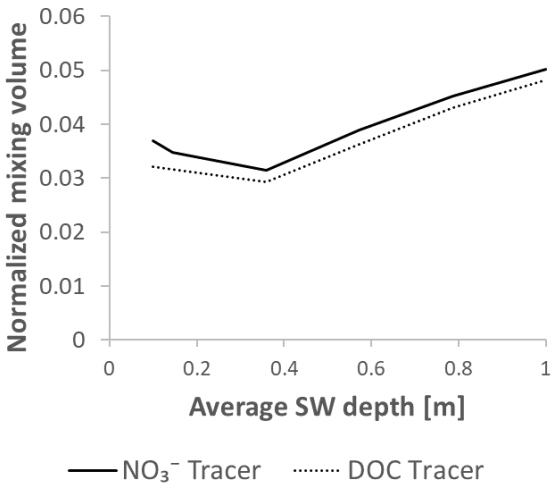

Figure 15: Response of hyporheic mixing zone volume to average surface water depth as measured by the size of the concentration gradient created by non-reactive tracers sourcing from the surface water and groundwater at the same concentrations as the reactive solutes (DOC and NO_3^-, where DOC was sourced from surface water and NO_3^- from groundwater). DOC=dissolved organic carbon, SW=surface water. We defined the mixing zone volume as the portion of the model domain with tracer concentrations between 10-90% of the constant input concentration [*Hester et al.*, 2013; *Pool et al.*, 2014; *Pool et al.*, 2015], then normalized to the model domain size.

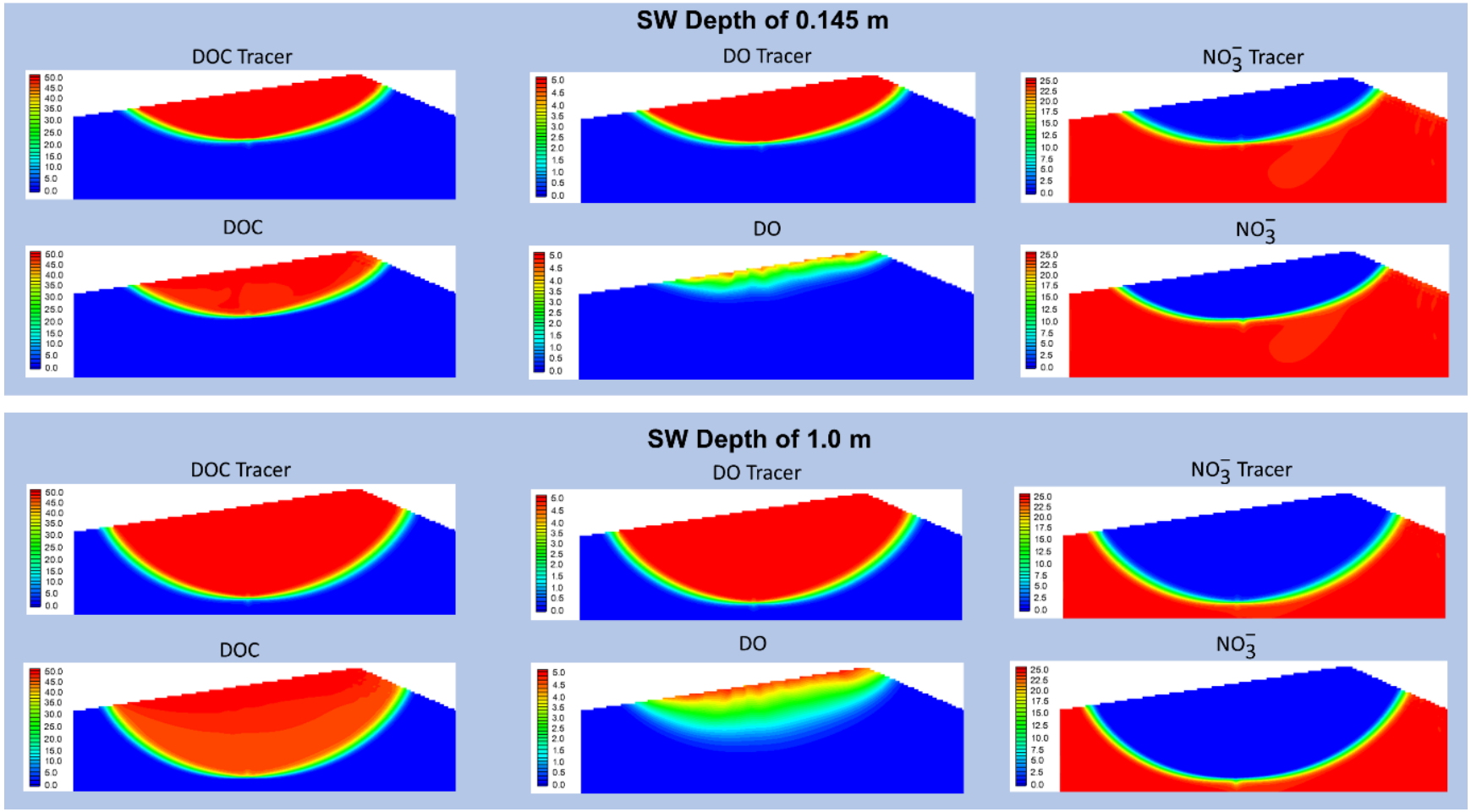

Figure 16: Response of the hyporheic mixing zone volume and flow cell depth at an average surface water depth of 0.145 m and 1.0 m in a homogeneous hydraulic conductivity field. Conservative tracers use the same boundary concentrations as the respective reactive component (DOC, DO, NO_3^-). Conservative tracer concentration plots are provided in addition to the reactive solutes to highlight the effect of the surface water depth on the volume and depth of the hyporheic flow cell and the mixing volume.

Introducing heterogeneity to the system led to a decrease in aerobic respiration (Figures 7ab, 9ab) which may be due to a slight decrease in the depth of the mixing cell (Figures 17 and 18). The trend in the depth of the stagnation point with surface water depth (Figure 18), used as an indicator for the depth of the hyporheic flow cell, follows a similar trend to the rate of both aerobic respiration and denitrification (Figure 6) as well as the normalized mixing zone volume (Figure 15). The depth of the stagnation point decreases until an inflection point is reached at a depth of about 0.40 m then increases with surface water depth. The decrease in the depth of the stagnation point in the heterogeneous system may be due to flow focusing, where residence times decrease when heterogeneity is introduced into groundwater flowpaths which in turn limits non-mixing dependent aerobic respiration [*Rolle et al.*, 2009; *Werth et al.*, 2006]. This would indicate kinetics limitation.

The homogeneous basecase had a decrease in average travel time of tracer particles in the upwelling groundwater to the dune surface of 14.7% from the lowest surface water depth to the highest; the heterogeneous basecase decreased by 12.0% (Figure 19). Using this average travel time as an indicator of residence time of groundwater in the mixing zone, we can conclude that mixing-dependent denitrification (Figure 6b) is transport limited, and in contrast to aerobic respiration, the decreased residence time (Figure 19) for the deeper surface water depth allows more nitrate to reach the mixing zone and undergo reaction. There is minimal difference in the trends in residence time between the homogeneous and heterogeneous cases, though the heterogeneous case generally has a larger standard deviation of the travel times for the groundwater tracer particles.

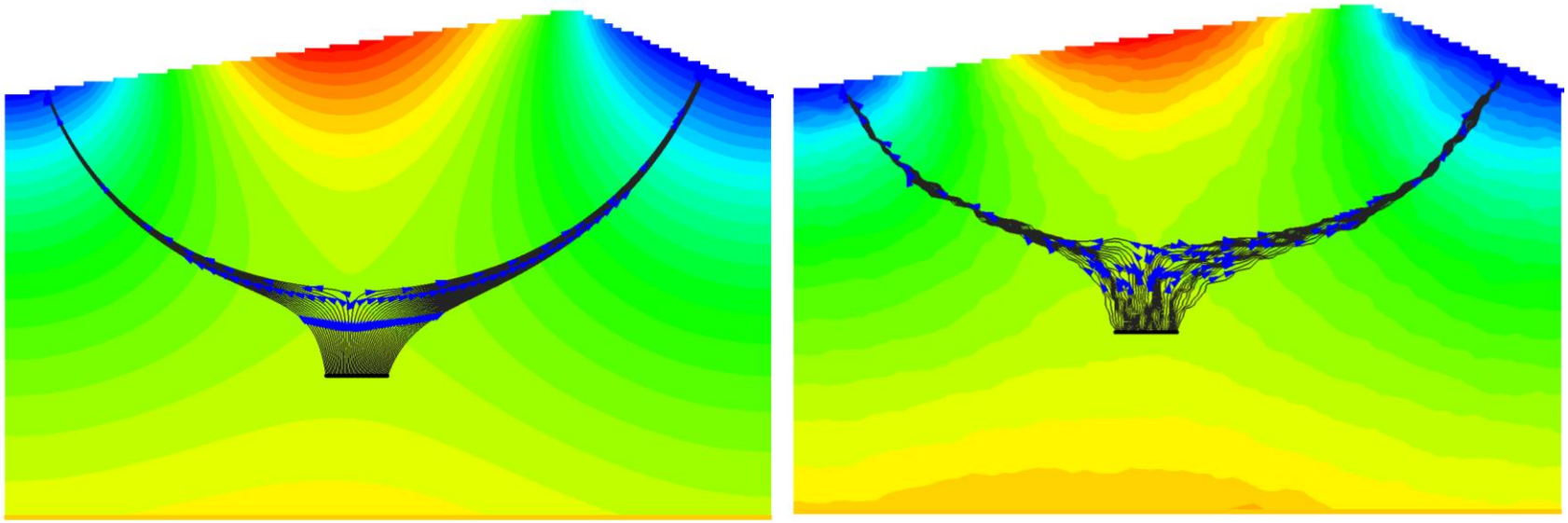

Figure 17: Comparison of MODPATH particle tracks through the equivalent homogeneous dune (84.4 m/d) and the heterogeneous basecase.

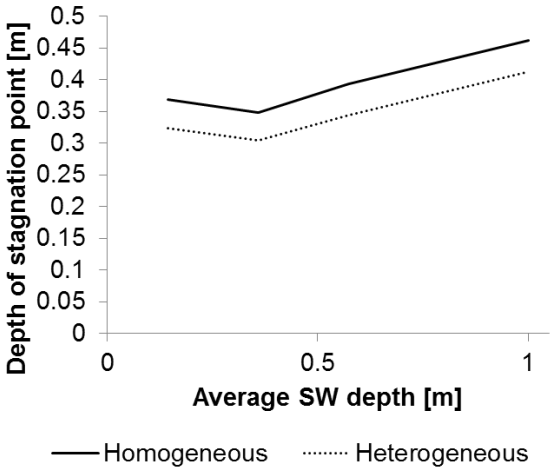

Figure 18: Comparison of the depth of the mixing zone as measured by the stagnation point for homogeneous and heterogeneous hydraulic conductivity fields. These are steady-state runs with varying average surface water depths. The depth of the stagnation point was measured by observing 45 tracer particles starting a standard distance directly under the deepest part of the mixing zone and determining the location at which the split in their travel paths in the positive and negative x-direction occurred.

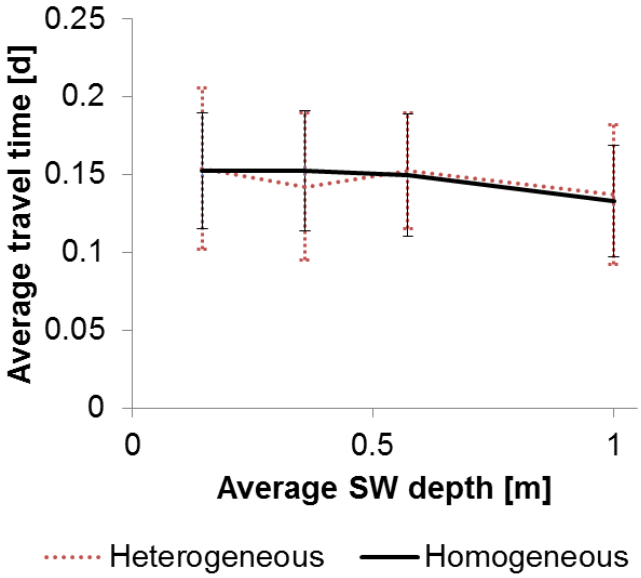

Figure 19: Residence times of the tracer particles tracked for the homogeneous and heterogeneous basecases in Figure 17 at varying surface water depths. These are steady-state runs with varying average surface water depths. The markers indicate the average travel time and error bars indicate the standard deviation of the travel time of each set of particles.

In our homogeneous unsteady results, neither the amplitude nor the period of surface water fluctuations much affected non-mixing dependent aerobic respiration and mixing-dependent denitrification (Figure 11, 12). This is in disagreement with *Shuai et al.* [2017], where daily fluctuations on a riverbank significantly increased denitrification. However, *Shuai et al.* [2017] sourced all reactants from surface water and included a nitrification reaction; the increase in amplitude increased residence time, likely providing additional anaerobic conditions for denitrification to occur. For our study, daily (short term) fluctuations had less effect on denitrification and aerobic respiration than longer-term fluctuations in surface water depth (compare Figures 5 and 11). Quantitatively, the difference between no fluctuation and the largest amplitude fluctuation is approximately 10.8% for oxygen consumption via aerobic respiration and approximately 4.3% for nitrate consumption via denitrification (Figure 11) compared to 270% and 78% for long term fluctuations (Figure 5). This is likely due to how the water levels in the fluctuating case (0.2-1.0 m depth, Figure 2c) map onto the steady state trend in aerobic respiration and denitrification versus surface water depths (Figure 5). In particular, for lower amplitudes the water levels oscillate within the nearly linear trend in reaction rates for depths 0.4 m to 1.0 m rather than reaching the elevated rates of reaction at depths shallower than the inflection point. In other words, the fluctuating surface water depth does not linger at either the highest or lowest depths that produce an increase in the rates of aerobic respiration and denitrification in the way that the instantaneous change does (Table 4). This also explains why the maximum amplitude tested *does* have an increase in both aerobic respiration and denitrification: it is the only amplitude tested that reaches these highest and lowest depths. Additionally, this explains why changing the period of the fluctuation did not affect the rates of aerobic respiration and denitrification (Figure 12); all of these conditions spend a similar amount of time at the highest and lowest depths.

The small effect of combining unsteady surface water condition with a heterogeneous field on changes in mass consumption due to aerobic respiration and denitrification was unexpected. We had expected the amount of denitrification to increase substantially as proposed by *Neeper* [2001] and *Hester et al.* [2017]. However, upon closer evaluation our results do not refute this hypothesis. In order to see these types of effects, the duration or period of fluctuations must be of a similar magnitude to the travel time of contaminants through pockets of lower hydraulic conductivity. Because the spatial scale of these pockets in our model are at most a few

centimeters and the lowest hydraulic conductivity is ~2 m/d, the fluctuation period would need to be on the order of 0.1 days to match the travel time of water through the pockets. Because our modeled fluctuation periods were intended to simulate common river fluctuations, their period was much longer, thereby reducing the effect. To better test the effect of daily surface water fluctuations on mixing-dependent reactions and hence the veracity of this theory, we would need to simulate larger scale heterogeneity with corresponding longer residence times, and hence the physical scale of our model would need to be larger.

2.4.2 Engineering applications

For hyporheic exchange induced by flow over riverbed ripples and dunes [*Elliott and Brooks*, 1997a,b; *Packman*, 2004], the residence time of solutes in the mixing zone and hyporheic flow cell size both scale with dune size. Dune size in turn scales with river size, and in large rivers like the Mississippi, dunes may be upwards of 20 m in length [*Harbor*, 1998], which may have increased potential for mixing-dependent reactions. Hyporheic exchange can also be driven by larger morphological forms such as cascades, riffles, and meanders [*Cardenas*, 2009a] and flow obstructions such as logs, boulders, weirs, or dams [*Hester et al.*, 2008; *Winter et al*., 1998]. Many of these forms create much larger flow cells than this study considers and would have greater non-mixing dependent and mixing dependent reactions occurring within the flow cell and mixing zone, respectively. This greater effect would be on a per flow cell basis, yet due to their greater size there may be fewer flow cells per unit length or area of river, and hence the net effect is unknown.

Nevertheless, river restoration or management efforts that create these types of bedforms and flow obstructions could enhance both mixing-dependent and non-mixing dependent beneficial hyporheic reactions. A number of prior studies have advocated active intervention in stream or river channels to create both surface and subsurface structures [*Herzog et al.*, 2016; *Hester et al.*, 2016; *Ward et al.*, 2011], yet more holistic approaches may also achieve similar results in the longer run. For example, restoring riparian forest buffers could restore channel migration [*Hester and Cranmer*, 2014], in turn allowing mature trees to periodically fall into the channel, creating in-stream structures. Directly creating dunes and ripples is likely not practical, but instead self-creation of dunes and ripples could be encouraged by daylighting buried streams

and recreating more natural sediment dynamics [*Elmore and Kaushal*, 2008]. Nevertheless, creation of hyporheic flow cells in the first place is heavily dependent on the hydrologic context of the river (e.g., gaining/losing conditions), which must be borne in mind [*Azinheira et al.*, 2014; *Hester et al.*, 2018].

The effects of river regulation on contaminant migration are worth considering. River regulation by hydroelectric dams typically induce daily and weekly cycles in surface water fluctuations where power is generated more during the middle of the day and middle of the week than at nights or weekends. They also induce seasonal cycles where more power is generated in seasons where greater heating or cooling needs exist [*Casas-Mulet et al.*, 2015]. Times of higher flooding may increase the amount of mixing-dependent reaction that takes place, provided that those reactions are transport limited.

Finally, mixing-dependent reactions of contaminants upwelling from groundwater to rivers in the hyporheic zone may the last line of defense before entering surface water. Contaminants in deeper groundwater may only encounter reactive conditions upon reaching the hyporheic zone, where other reactants from the surface water can intermingle. Thus, accounting for the potential mitigation effects of hyporheic mixing dependent reactions may be important to monitoring natural attenuation (MNA) effects at contaminated groundwater sites. MNA refers to the monitoring of the reduction of concentrations or mass flow rates of contaminants as they travel away from their source as a management practice for contaminated land and groundwater [*Rügner et al.*, 2006]. Mixing-dependent reactions are potentially critical in determining the fate of contaminants in groundwater plumes, and better inform MNA practices.

2.4.3 Sources of uncertainty

Our model assumed only one form of organic carbon was present in the form of labile DOC and only considered one set of contaminant boundary conditions. In actual rivers, the carbon sources available to undergo reaction are much more diverse and the concentrations of solutes in the surface water and groundwater are subject to spatial and temporal variability. Additionally, we did not account for spatial or temporal variance in microbial reaction rates.

We were limited in the range of depths that we were able to test by both the model domain and the ranges used in *Fehlman* [1985] to develop the relation between surface water depth and the pressure distribution across the dune (Equation 12). Higher surface water depths than those tested would have resulted in hyporheic flow cells with edges that would realistically fall beyond the no flow boundaries upstream and downstream of the dune. In addition, the relation developed by *Fehlman* [1985] is based on empirical data for H/d of 0.1 to 0.7.

All heterogeneous fields used were generated during previous work [*Hester et al*., 2013; *Hester et al.*, 2014]. We limited the ranges of heterogeneity parameters that we tested to these formerly generated fields. Nevertheless, those formerly generated fields were constrained by more fundamental limitations, for example higher variance heterogeneous fields presented unreasonable runtimes for higher surface water depths. Similarly, the correlation length of the heterogeneous fields could not be increased much without violating the ergodicity assumption. Increasing the correlation length thus would require increasing the model domain size, which was not possible without sacrificing grid cell resolution, the latter being necessary to minimize numerical dispersion, which is critical for accurately simulating mixing-dependent reactions.

We only considered the aqueous phase of solutes and did not account for retardation due to sorption. While the effects of this are negligible for the steady-state model [*Marzadri et al.*, 2011; *Zarnetske et al.*, 2012], the introduction of this aspect into the solute transport model would most likely increase the amount of mixing-dependent denitrification taking place for the unsteady conditions, most notably unsteady surface water conditions on heterogeneous fields. This may provide additional explanation as to why we saw unsteady conditions on a heterogeneous field have a smaller impact than expected.

2.5 Conclusions

We modelled riverbed dune-induced hyporheic exchange between surface water and upwelling groundwater and quantified mixing-dependent denitrification for a set of varied hydraulic conditions (Table 1). Solute boundary conditions were specified to ensure that all aerobic respiration occurring in the system was non-mixing dependent and all denitrification occurring was mixing-dependent. Overall, we found that both the amount of mixing-dependent

and non-mixing dependent reaction increased with steady state surface water depth, but the effects of daily surface water fluctuations were comparatively minor.

We first varied steady-state surface water depths from 0.10 m to 1.0 m on homogeneous sediment. As surface water depth increased, non-mixing dependent aerobic respiration increased by 270% and mixing-dependent denitrification increased by 78% once depths exceeded an inflection point at a depth of 0.4 m (Figure 5ab). When we applied the same surface water conditions to heterogeneous hydraulic conductivity fields, we found very similar responses to changes in surface water depth (Figure 6). As horizontal correlation length increased from 0 to 9 cm percent of DO consumed decreased by ~6% and percent of NO_3^- consumed exhibited a net increase of ~4.7% for each surface water depth. As variance of the heterogeneous hydraulic conductivity field increased from 0 to 1.0, percent of DO consumed decreased by ~20% for all surface water depths, and percent of NO_3^- consumed varied by ~0.5%.

We then varied unsteady surface water conditions in homogeneous sediment. As the amplitude of daily sinusoidal SW fluctuations increased from 0.0 to 0.4m, DO consumption through aerobic respiration increased by 10.8% and nitrate consumption through denitrification increased by only 4.3% (Figure 11ab). When testing the effect of the rate of change, we found that the 24-hour 0.4725 m amplitude sinusoidal fluctuation had higher levels of aerobic respiration and denitrification than the steady-state average depth value by 16% for DO and 7.5% for NO_3^-, and the instantaneous change had slightly higher levels than the sinusoidal change, 19% for DO and 9.8% for NO_3^- (Table 3). A more dramatic and sudden change in surface water depth increased the amount of both aerobic respiration and denitrification relative to a more gradual fluctuation. For unsteady conditions, because of the nonlinearity (inflection) in the relationship between SW depth and pressure drag across the dune, the amount of simulation time spent at the lowest (0.145 m) and highest SW depths (1.0 m) with higher rates of reaction can outweigh lower reaction rates for time spent at the inflection point at intermediate depth (0.4 m).

Maximizing the effects of mixing-dependent reactions is a function of the residence time in the hyporheic flow cell. Larger dunes or alternative sources of hyporheic exchange, such as riffle-pools or obstructions to river flow, may induce larger hyporheic flow cells and therefore longer mixing zones, more mixing, and more mixing-dependent reaction on an individual flow

cell basis. The net effect on solute or pollutant transport in a river corridor would then depend on the number of such cells present and the surface flow in the channel. Mixing-dependent reactions in the hyporheic zone are an important function of river systems. Some contaminants in deeper groundwater may only encounter reactive conditions upon reaching the hyporheic zone, where other reactants from the surface water can intermingle. Because mixing-dependent reactions exist as a potentially important source for groundwater remediation, it is important to develop better understanding of which parameters affect these reactions and in what ways.

References

Anderson, W. P., Storniolo, R. E., & Rice, J. S. (2011). Bank thermal storage as a sink of temperature surges in urbanized streams. *Journal of Hydrology*, *409*(1–2), 525–537. https://doi.org/10.1016/j.jhydrol.2011.08.059

Azinheira, D. L., D. T. Scott, W. C. Hession, and E. T. Hester. 2014. Comparison of effects of inset floodplains and hyporheic exchange induced by in-stream structures on solute retention. Water Resources Research 50:6168-6190.

Bardini, L., Boano, F., Cardenas, M. B., Revelli, R., & Ridolfi, L. (2012). Nutrient cycling in bedform induced hyporheic zones. *Geochimica et Cosmochimica Acta*, *84*, 47–61. https://doi.org/10.1016/j.gca.2012.01.025

Bauer, R. D., Rolle, M., Bauer, S., Eberhardt, C., Grathwohl, P., Kolditz, O. Griebler, C. (2009). Enhanced biodegradation by hydraulic heterogeneities in petroleum hydrocarbon plumes. *Journal of Contaminant Hydrology*, *105*(1–2), 56–68. https://doi.org/10.1016/j.jconhyd.2008.11.004

Bianchin, M. S., Smith, L., & Beckie, R. D. (2011). Defining the hyporheic zone in a large tidally influenced river. *Journal of Hydrology*, *406*(1–2), 16–29. https://doi.org/10.1016/j.jhydrol.2011.05.056

Boano, F., Demaria, A., Revelli, R., & Ridolfi, L. (2010). Biogeochemical zonation due to intrameander hyporheic flow. *Water Resources Research*, *46*(2), 1–13. https://doi.org/10.1029/2008WR007583

Braun, E. (2007). *Reactive nitrogen in the environment: too much or too little of a good thing.* Paris; Falmouth, MA: UNEP DTIE, Sustainable Consumption and Production (SCP) Branch ; Woods Hole Research Center.

Brunke, M., & Gonser, T. (1997). The ecological significance of exchange processes between rivers and groundwater. *Freshwater Biology*, *37*(1), 1–33. https://doi.org/10.1046/j.1365-2427.1997.00143.x

Cardenas, M. B. (2009). Stream-aquifer interactions and hyporheic exchange in gaining and losing sinuous streams. *Water Resources Research*, *45*(6), 1–13. https://doi.org/10.1029/2008WR007651

Cardenas, M. B. (2009). A model for lateral hyporheic flow based on valley slope and channel sinuosity. *Water Resources Research*, *45*(1), 1–5. https://doi.org/10.1029/2008WR007442

Cardenas, M. B., and J. L. Wilson. 2006. The influence of ambient groundwater discharge on exchange zones induced by current-bedform interactions. *Journal of Hydrology* **331**:103-109.s

Cardenas, M. B., & Wilson, J. L. (2007). Hydrodynamics of coupled flow above and below a sediment-water interface with triangular bedforms. *Advances in Water Resources*, *30*(3), 301–313. https://doi.org/10.1016/j.advwatres.2006.06.009

Castro-Alcalá, E., Fernaàndez-Garcia, D., Carrera, J., & Bolster, D. (2012). Visualization of mixing processes in a heterogeneous sand box aquifer. *Environmental Science and Technology*, *46*(6), 3228–3235. https://doi.org/10.1021/es201779p

Cirpka, O. A., Frind, E. O., & Helmig, R. (1999). Numerical simulation of biodegradation controlled by transverse mixing. *Journal of Contaminant Hydrology*, *40*(2), 159–182. https://doi.org/10.1016/S0169-7722(99)00044-3

Conant, B., Cherry, J. A., & Gillham, R. W. (2004). A PCE groundwater plume discharging to a river: Influence of the streambed and near-river zone on contaminant distributions. *Journal of Contaminant Hydrology*, *73*(1–4), 249–279. https://doi.org/10.1016/j.jconhyd.2004.04.001

Dubrovsky, N. M., Burow, K. R., Clark, G. M., Gronberg, J. M., Hamilton, P. A., Hitt, K. J., … Wilber, W. G. (2010). *The quality of our Nation's waters-Nutrients in the Nation's streams and groundwater, 1992-2004*. *Circular*. Retrieved from http://pubs.er.usgs.gov/publication/cir1350

Dudley-Southern, M., & Binley, A. (2015). Temporal responses of groundwater-surface water exchange to successive storm events. *Water Resources Research*, *51*(2), 1112–1126. https://doi.org/10.1002/2014WR016623

Duff, J. H., & Triska, F. J. (1990). Denitrification in sediments from the hyporheic zone adjacent to a small forested stream. *Canadian Journal of Fisheries and Aquatic Sciences*, *47*(6), 1140–1147. https://doi.org/10.1139/f90-133

Elliott, H., & Brooks, N. H. (1997). Transfer of nonsorbing solutes to a streambed with bed forms: Laboratory experiments. *Water Resources Research*, *33*(1), 137–151.

Elliott, H., & Brooks, N. H. (1997). Transfer of nonsorbing solutes to a streambed with bed forms : Theory. *Water Resources Research*, *33*(1), 123–136.

Elmore, A. J., and S. S. Kaushal. 2008. Disappearing headwaters: patterns of stream burial due to urbanization. Frontiers in Ecology and the Environment 6:308-312.

Fehlman, H. M. (1985). Resistance components and velocity distributions of open channel flows over bedforms (Thesis).

Fitts, Charles R. (2013) *Groundwater Science (Second Edition)*, Boston: Academic Press. https://doi.org/10.1016/B978-0-12-384705-8.00001-7.

Gomez-Velez, J. D., Harvey, J. W., Cardenas, M. B., & Kiel, B. (2015). Denitrification in the Mississippi River network controlled by flow through river bedforms. *Nature Geoscience*, *8*(12), 941–945. https://doi.org/10.1038/ngeo2567

Gu, C., Anderson, W., & Maggi, F. (2012). Riparian biogeochemical hot moments induced by stream fluctuations. *Water Resources Research*, *48*(9), 1–17. https://doi.org/10.1029/2011WR011720

Harbor, D. J. (1998). Dynamics of bedforms in the lower mississippi river SEPM - Society for Sedimentary Geology. doi:10.2110/jsr.68.750

Harvey, J. W., Böhlke, J. K., Voytek, M. A., Scott, D., & Tobias, C. R. (2013). Hyporheic zone denitrification: Controls on effective reaction depth and contribution to whole-stream mass balance. *Water Resources Research*, *49*(10), 6298–6316. https://doi.org/10.1002/wrcr.20492

Harvey, J. W., & Wagner, B. J. (2000). *Quantifying Hydrologic Interactions Between Streams and Their Subsurface Hyporheic Zones*. *Streams and Ground Waters*. https://doi.org/10.1016/B978-012389845-6/50002-8

Herzog, S. P., C. P. Higgins, and J. E. McCray. (2016). Engineered Streambeds for Induced Hyporheic Flow: Enhanced Removal of Nutrients, Pathogens, and Metals from Urban Streams. Journal of Environmental Engineering 142.

Hester, E. T., and E. N. Cranmer. (2014). Variation of hyporheic exchange potential among urban streams and implications for stream restoration. *Environmental and Engineering Geoscience* 20:287-304.

Hester, E. T., K. E. Brooks, and D. T. Scott. (2018). Comparing reach scale hyporheic exchange and denitrification induced by instream restoration structures and natural streambed morphology. Ecological Engineering 115:105-121.

Hester, E. T., Young, K. I., & Widdowson, M. A. (2013). Mixing of surface and groundwater induced by riverbed dunes: Implications for hyporheic zone definitions and pollutant reactions. *Water Resources Research*, *49*(9), 5221–5237. https://doi.org/10.1002/wrcr.20399

Hester, E. T., B. Hammond, and D. T. Scott. (2016). Effects of inset floodplains and hyporheic exchange induced by in-stream structures on nitrate removal in a headwater stream. *Ecological Engineering* 97:452-464.

Hester, E. T., & Doyle, M. W. (2008). In-stream geomorphic structures as drivers of hyporheic exchange. *Water Resources Research*, *44*(3). https://doi.org/10.1029/2006WR005810

Hester, E. T., Young, K. I., & Widdowson, M. A. (2014). Controls on mixing-dependent denitrification in hyporheic zones induced by riverbed dunes: A steady state modeling

study. *Water Resources Research*, *50*(11), 9048–9066. https://doi.org/10.1002/2014WR015424

Hester, E. T., Cardenas, M. B., Haggerty, R., & Apte, S. V. (2017). The importance and challenge of hyporheic mixing. *Water Resources Research*, *53*, 3565–3575. https://doi.org/10.1002/2016WR020005

Hill, A. R., & Lymburner, J. (1998). Hyporheic zone chemistry and stream-subsurface exchange in two groundwater-fed streams. *Canadian Journal of Fisheries and Aquatic Sciences*, *55*(1996), 495–506. https://doi.org/10.1139/f97-250

Hopkinson, L. C., & Walburn, C. Z. (2016). Near-boundary velocity and turbulence in depth-varying stream flows. *Environmental Fluid Mechanics*, *16*(3), 559–574. https://doi.org/10.1007/s10652-015-9440-1

Huang, F. K., Chuang, M. H., Wang, G. S., & Yeh, H. Der. (2015). Tide-induced groundwater level fluctuation in a U-shaped coastal aquifer. *Journal of Hydrology*, *530*, 291–305. https://doi.org/10.1016/j.jhydrol.2015.09.032

Kennedy, C. D., Genereux, D. P., Corbett, D. R., & Mitasova, H. (2009). Relationships among groundwater age, denitrification, and the coupled groundwater and nitrogen fluxes through a streambed. *Water Resources Research*, *45*(9), 1–15. https://doi.org/10.1029/2008WR007400

Landmeyer, J. E., Bradley, P. M., Trego, D. A., Hale, K. G., & Haas, J. E. (2010). MTBE, TBA, and TAME attenuation in diverse hyporheic zones. *Ground Water*, *48*(1), 30–41. https://doi.org/10.1111/j.1745-6584.2009.00608.x

Lin, Y. C., & Medina, M. A. (2003). Incorporating transient storage in conjunctive stream-aquifer modeling. *Advances in Water Resources*, *26*(9), 1001–1019. https://doi.org/10.1016/S0309-1708(03)00081-2

Loheide, S. P., & Lundquist, J. D. (2009). Snowmelt-induced diel fluxes through the hyporheic zone. *Water Resources Research*, *45*(7), 1–9. https://doi.org/10.1029/2008WR007329

Maggi, F., C. Gu, W. Riley, G. Hornberger, R. Venterea, T. Xu, N. Spycher, C. Steefel, N. Miller, and C. Oldenburg (2008), A mechanistic treatment of the dominant soil nitrogen cycling processes: Model development, testing, and application, *Journal of Geophysical Research: Biogeosciences (2005–2012)*, 113(G2).

Malzone, J. M., Lowry, C. S., & Ward, A. S. (2016). Response of the hyporheic zone to transient groundwater fluctuations on the annual and storm event time scales. *Water Resources Research*, *52*(7), 5301–5321. https://doi.org/10.1002/2015WR018056

Marzadri, A., Tonina, D., Bellin, A., & Valli, A. (2016). Mixing interfaces, fluxes, residence times and redox conditions of the hyporheic zones induced by dune-like bedforms and ambient groundwater flow. Elsevier.

McCallum, J. L., Cook, P. G., Brunner, P., & Berhane, D. (2010). Solute dynamics during bank storage flows and implications for chemical base flow separation. *Water Resources Research*, *46*(7), 1–12. https://doi.org/10.1029/2009WR008539

McCallum, J. L., & Shanafield, M. (2016). Residence times of stream-groundwater exchanges due to transient stream stage fluctuations. *Water Resources Research*, *52*(3), 2059–2073. https://doi.org/10.1002/2015WR017441

Moser, D. P., Fredrickson, J. K., Geist, D. R., Arntzen, E. V., Peacock, A. D., Li, S. M. W., … McKinley, J. P. (2003). Biogeochemical Processes and Microbial Characteristics across Groundwater-Surface Water Boundaries of the Hanford Reach of the Columbia River. *Environmental Science and Technology*, *37*(22), 5127–5134. https://doi.org/10.1021/es034457v

Naranjo, R. C., Niswonger, R. G., & Davis, C. J. (2015). Mixing effects on nitrogen and oxygen concentrations and the relationship to mean residence time in a hyporheic zone of a riffle-pool sequence. *Water Resources Research*, *51*(9), 7202–7217. https://doi.org/10.1002/2014WR016259

Neeper, D. A. (2001). A model of oscillatory transport in granular soils, with application to barometric pumping and earth tides. *Elsevier*. doi:10.1016/S0169-7722(00)00181-9

Packman, A. I., Salehin, M., & Zaramella, M. (2004). Hyporheic Exchange with Gravel Beds: Basic Hydrodynamic Interactions and Bedform-Induced Advective Flows. *Journal of Hydraulic Engineering*, *130*(7), 647–656. https://doi.org/10.1061/(ASCE)0733-9429(2004)130:7(647)

Peralta-Maraver, I., Reiss, J., & Robertson, A. L. (2018). Interplay of hydrology, community ecology and pollutant attenuation in the hyporheic zone. *Science of the Total Environment*, *610–611*, 267–275. https://doi.org/10.1016/j.scitotenv.2017.08.036

Pool, M., Post, V. E. A., & Simmons, C. T. (2015). Effects of tidal fluctuations and spatial heterogeneity on mixing and spreading in spatially heterogeneous coastal aquifers. *Water Resources Research*, *51*(3), 1570–1585. https://doi.org/10.1002/2014WR016068.Received

Pool, M., Post, V. E. A., & Simmons, C. T. (2014). Effects of tidal fluctuations on mixing and spreading in coastal aquifers: Homogeneous case. *Water Resources Research*, *50*(8), 6910–6926. https://doi.org/10.1002/2014WR015534.

Raudkivi, A. J. (1963). Study of Sediment Ripple Formation. *ASCE, Journal of Hydraulics Division*, *89*(6). 15-34.

Rifai, M. F., & Smith, K. V. H. (1969). Discussion of "Pressure Fluctuations in Reattaching Flow," by R. Narayanan and A. J. Reynolds. (ASCE, Proc. Paper 6212). *ASCE* 89(5).

Rolle, M., C. Eberhardt, G. Chiogna, O. A. Cirpka, and P. Grathwohl. 2009. Enhancement of dilution and transverse reactive mixing in porous media: Experiments and model-based interpretation. Journal of Contaminant Hydrology **110**:130-142.

Rügner, H., Finkel, M., Kaschl, A., & Bittens, M. (10/2006). Application of monitored natural attenuation in contaminated land management—A review and recommended approach for Europe. *Elsevier*. doi:10.1016/j.envsci.2006.06.001

Sawyer, A. H., Cardenas, M. B., Bomar, A., & Mackey, M. (2009). Impact of dam operations on hyporheic exchange in the riparian zone of a regulated river. *Hydrological Processes*, *23*, 2129–2137. https://doi.org/10.1002/hyp7324

Schmadel, N. M., Ward, A. S., Lowry, C. S., & Malzone, J. M. (2016). Hyporheic exchange contolled by dynamic hydrologic boundary conditions. *Geophysical Research Letters*, 1–10. https://doi.org/10.1002/2016GL068286.

Shuai, P., Cardenas, M. B., Knappett, P. S. K., Bennett, P. C., & Neilson, B. T. (2017). Denitrification in the banks of fluctuating rivers: The effects of river stage amplitude, sediment hydraulic conductivity and dispersivity, and ambient groundwater flow. *American Geophysical Union*. doi:10.1002/2017WR020610

Sinha, S., Hardy, R. J., Blois, G., Best, J. L., & Smith, G. H. S. (2017). Permeability on Determining Flow Structures Over River Dunes. *Water Resources Research*, *53*(4), 3067–3086. https://doi.org/10.1002/2016WR019662.

Smith, R. L., and Duff, J. H. (1988). 'Denitirification in a sand and gravel aquifer. *Appl. Environ. Microbiology*, 54(5), 1071–1078.

Spanning, R. J. M., Richardson, D. J., & Ferguson, S. J. (2007). Chapter 1 - Introduction to the Biochemistry and Molecular Biology of Denitrification. In H. Bothe, S. J. Ferguson, & W. E. Newton (Eds.), *Biology of the Nitrogen Cycle* (pp. 3–20). Amsterdam: Elsevier. https://doi.org/10.1016/B978-044452857-5.50002-3

Squillace, P. J., Thurman, E. M., & Furlong, E. T. (1993). Groundwater As a Nonpoint-Source of Atrazine and Deethylatrazine in a River During Base-Flow Conditions. *Water Resources Research*, *29*(6), 1719–1729.

Squillace, P. J. (1996). Observed and simulated movement of bank-storage water. *Ground Water*, *34*(1), 121–134. https://doi.org/10.1111/j.1745-6584.1996.tb01872.x

Triska, F. J., Kennedy, V. C., Avanzino, R. J., Zellweger, G. W., & Bencala, K. E. (1989). Retention and Transport of Nutrients in a Third-Order Stream in Northwestern California : Hyporheic Processes. *Ecology*, *70*(6), 1893–1905.

Vanoni, V. A., & Hwang, L. S. (1967). Relation Between Bed Forms and Friction in Streams. *ASCE, Journal of Hydraulics Division.*

Vittal, N., Ranga Raju, K. G., & Garde, R. J. (1977). Resistance of Two-Dimensional Triangular Roughness. *Journal of Hydraulic Research*. 15(1).

Wang, W. C. (1983). Flow Characteristics Over Alluvial Bedforms. Ph.D. Dissertation. *Colorado State University.*

Ward, A. S., M. N. Gooseff, and P. A. Johnson. 2011. How can subsurface modifications to hydraulic conductivity be designed as stream restoration structures? Analysis of Vaux's conceptual models to enhance hyporheic exchange. *Water Resources Research* 47:W08512

Werth, C. J., O. A. Cirpka, and P. Grathwohl. 2006. Enhanced mixing and reaction through flow focusing in heterogeneous porous media. *Water Resources Research* 42:W12414.

White, D. S. (1993). Perspectives on defining and delineating hyporheic zones. *Journal of the North American Benthological Society*, *12*(1), 61–69.

Winter, T. C., Harvey, J. W., Franke, O. L., & Alley, W. M. (1998). Ground water and surface water: A single resource. *USGS Publications*, 79. https://doi.org/10.3389/fpsyg.2012.00044

Zarnetske, J. P., Haggerty, R., Wondzell, S. M., & Baker, M. A. (2011). Dynamics of nitrate production and removal as a function of residence time in the hyporheic zone. *Journal of Geophysical Research: Biogeosciences*, *116*(1), 1–12. https://doi.org/10.1029/2010JG001356

Zarnetske, J. P., Haggerty, R., Wondzell, S. M., Bokil, V. A., & González-Pinzón, R. (2012). Coupled transport and reaction kinetics control the nitrate source-sink function of hyporheic zones. *Water Resources Research*, *48*(11), 1–15. https://doi.org/10.1029/2012WR011894

Zimmer, M. A., & Lautz, L. K. (2014). Temporal and spatial response of hyporheic zone geochemistry to a storm event. *Hydrological Processes*, *28*(4), 2324–2337. https://doi.org/10.1002/hyp.9778

3. Engineering Applications

The residence time of solutes in the mixing zone and hyporheic cell size scale with dune size, and dunes scale with river size. In large rivers like the Mississippi, dunes may be upwards of 20 m in length [*Harbor*, 1998] and may have more potential for mixing-dependent reactions. Hyporheic exchange can also be driven flow over riverbed ripples and dunes [*Elliott and Brooks*, 1997a,b; *Packman*, 2004]; larger morphological forms such as cascades, riffles, and meanders [*Cardenas*, 2009]; and flow obstructions such as logs, boulders, weirs, or dams [*Hester et al.*, 2008; *Winter et al*., 1998]. Many of these bedforms create much larger flow cells than this study considers and would increase both non-mixing dependent reactions in the flow cell and mixing dependent reactions in the mixing zone. River restoration efforts could focus on creating these types of bedforms and flow obstructions in order to induce hyporheic exchange and encourage denitrification, both mixing-dependent and non-mixing dependent.

The effects of river regulation are worth considering. River regulation by hydroelectric dams typically induce daily and weekly cycles in surface water fluctuations where power is generated more during the middle of the day and middle of the week than at nights or weekends. They also induce seasonal cycles where more power is generated in seasons where greater heating or cooling needs exist [*Casas-Mulet et al.*, 2015]. Times of higher flooding will increase the amount of mixing-dependent reaction that takes place, provided that those reactions are transport limited. This knowledge could potentially be used in conjunction with records of times of increased loading of reactive solutes to better mitigate contaminants and control water quality.

Estimating of the amount of denitrification occurring in river systems is important for monitoring water quality. The microbial conversion of nitrate to N_2 in hyporheic zone is an important contributor to overall denitrification in rivers, streams and estuaries [*Duff and Triska*, 1990; *Gomez-Valez et al.*, 2015; *Hill and Lymburner*, 1998; *Triska et al.*, 1989; *Zarnetske*, 2011]. The runoff of nitrate from agricultural processes affects riverine wildlife and it is important to be able to accurately predict and monitor its concentration. These principles also apply to a range of other water borne contaminants.

Finally, mixing-dependent reactions of contaminants upwelling from groundwater to rivers in the hyporheic zone may the last line of defense before entering surface water.

Contaminants in deeper groundwater may only encounter reactive conditions upon reaching the hyporheic zone, where other reactants from the surface water can intermingle. Thus, accounting for the potential mitigation effects of hyporheic mixing dependent reactions may be important to monitoring natural attenuation (MNA) effects at contaminated groundwater sites. MNA refers to the monitoring of the reduction of concentrations or mass flow rates of contaminants as they travel away from their source [*Rügner et al.*, 2006]. Natural attenuation is a cost-effective method of remediation that may reduce the amount or concentration of the contaminant, or alternatively bind the contaminant to the soil and prevent further spread. It has been shown that natural attenuation can clean soil of hydrocarbons and BTEX pollutants [*Hejazi*, 2002], and it could be used as a management practice for contaminated land and groundwater [*Rügner et al.*, 2006]. Mixing-dependent reactions are potentially critical in determining the fate of contaminants in groundwater plumes, and better inform MNA practices.

References

Cardenas, M. B. (2009). Stream-aquifer interactions and hyporheic exchange in gaining and losing sinuous streams. *Water Resources Research*, *45*(6), 1–13. https://doi.org/10.1029/2008WR007651

Casas-Mulet, R., Alfredsen, K., Hamududu, B., & Timalsina, N. P. (2015). The effects of hydropeaking on hyporheic interactions based on field experiments THE EFFECT OF HYDROPEAKING ON HYPORHEIC INTERACTIONS John Wiley & Sons Inc. doi:10.1002/hyp.10264

Duff, J. H., & Triska, F. J. (1990). Denitrification in sediments from the hyporheic zone adjacent to a small forested stream. *Canadian Journal of Fisheries and Aquatic Sciences*, *47*(6), 1140–1147. https://doi.org/10.1139/f90-133

Elliott, H., & Brooks, N. H. (1997). Transfer of nonsorbing solutes to a streambed with bed forms: Laboratory experiments. *Water Resources Research*, *33*(1), 137–151.

Elliott, H., & Brooks, N. H. (1997). Transfer of nonsorbing solutes to a streambed with bed forms : Theory. *Water Resources Research*, *33*(1), 123–136.

Gomez-Velez, J. D., Harvey, J. W., Cardenas, M. B., & Kiel, B. (2015). Denitrification in the Mississippi River network controlled by flow through river bedforms. *Nature Geoscience*, *8*(12), 941–945. https://doi.org/10.1038/ngeo2567

Harbor, D. J. (1998). Dynamics of bedforms in the lower mississippi river SEPM - Society for Sedimentary Geology. doi:10.2110/jsr.68.750

Hejazi, R.F., 2002. Oily Sludge Degradation Study Under Arid Conditions Using a Combination of Landfarm and Bioreactor Technologies. PhD thesis, Faculty of Engineering and Applied Science, Memorial University of Newfoundland, St John's, Canada.

Hester, E. T., & Doyle, M. W. (2008). In-stream geomorphic structures as drivers of hyporheic exchange. *Water Resources Research*, *44*(3). https://doi.org/10.1029/2006WR005810

Hill, A. R., & Lymburner, J. (1998). Hyporheic zone chemistry and stream-subsurface exchange in two groundwater-fed streams. *Canadian Journal of Fisheries and Aquatic Sciences*, *55*(1996), 495–506. https://doi.org/10.1139/f97-250

Packman, A. I., Salehin, M., & Zaramella, M. (2004). Hyporheic Exchange with Gravel Beds: Basic Hydrodynamic Interactions and Bedform-Induced Advective Flows. *Journal of Hydraulic Engineering*, *130*(7), 647–656. https://doi.org/10.1061/(ASCE)0733-9429(2004)130:7(647)

Rügner, H., Finkel, M., Kaschl, A., & Bittens, M. (10/2006). Application of monitored natural attenuation in contaminated land management—A review and recommended approach for europe Elsevier. doi:10.1016/j.envsci.2006.06.001

Triska, F. J., Kennedy, V. C., Avanzino, R. J., Zellweger, G. W., & Bencala, K. E. (1989). Retention and Transport of Nutrients in a Third-Order Stream in Northwestern California : Hyporheic Processes. *Ecology*, *70*(6), 1893–1905.

Winter, T. C., Harvey, J. W., Franke, O. L., & Alley, W. M. (1998). Ground water and surface water: A single resource. *USGS Publications*, 79. https://doi.org/10.3389/fpsyg.2012.00044

Zarnetske, J. P., Haggerty, R., Wondzell, S. M., & Baker, M. A. (2011). Dynamics of nitrate production and removal as a function of residence time in the hyporheic zone. *Journal of Geophysical Research: Biogeosciences*, *116*(1), 1–12. https://doi.org/10.1029/2010JG001356

Appendix A: Using GMS Files

A.1 Hydraulic Boundary Conditions

- The upper boundary condition is a transient specified head.
    - 20 nodes across the dune
    - MODFLOW interpolates the head values between nodes
    - MODFLOW also interpolates the head values between the timesteps of the specified head inputs. To implement an instantaneous change, one must input overlapping head values at a timestep, i.e. [0.5 d, 0.45 m] and [0.5 d, 1.0 m].
    - To change, one must change the set of time-dependent head conditions and timestep series at each node. These timesteps must align with the timesteps used in "MODFLOW"->"Global Parameters"
- The bottom boundary is a constant flow boundary.
    - This can also be made transient, although we did not do so in this study
    - To change, one must change the constant flow value of this boundary
- The side boundaries are no flow boundaries.
- All implemented hydraulic changes must "map to" MODFLOW. To do this, right-click the coverage (it helps to rename the coverage each time with the test you are running), go to "Map to" and then click "MODFLOW/MODPATH"

A.2 MODFLOW

- Hydraulic conductivity can be changed in the "MODFLOW" section of the navigation bar under "LPF- Layer Property Flow"
- To change, open the LPF menu and click "Hydraulic Conductivity". To create a homogeneous field, go to "Constant Grid" and enter the new hydraulic conductivity value. To enter a heterogeneous field, copy and paste the desired field into the grid.
- To see the layout of the hydraulic conductivity field, to the file in the sidebar under the "MODFLOW" folder labeled "HK"

A.3 SEAM3D

- Boundary conditions are entered into the "Source/Sink Mixing Package" under the "SEAM3D" tab of the navigation bar. The surface water conditions were specified as constant head values and the groundwater conditions were entered as "well" type of conditions.
- Monod Kinetic inputs are entered using the "Biodegradation Package" under the "SEAM3D" tab.
- Dispersivity values are entered using the "Dispersion Package" under the "SEAM3D" tab.
- Initial concentrations: "Basic Transport Package" -> "Starting Conc. Per cell" click dots

Appendix B: R Scripts

B.1 Hydraulic boundary condition

```
#adjustable inputs – time-averaged depth and amplitude of fluctuation
avgdepth= .6
amplitude= 0.1

t= c(0,.1,.2,.3,.4,.5,.6,.7,.8,.9,1,1.1,1.2,1.3,1.4,1.5,1.6,1.7,1.8,1.9,2.0)


#multiply in sine function by 0.5 for 48hr period, 1 for 24hr, 2 for 12hr
timedep_avgdepth= amplitude*sin(1*2*3.14159*t) + avgdepth                #Eqn 10

xcoord= c(0,.05,0.1,0.15,0.2,0.27584,0.35,0.42489,0.5,0.57577,0.62271,0.6761,
    0.71506,0.74981,0.78181,0.81656,0.848878,0.88636,0.9144)             #locations of nodes


#manning's and other inputs
H=0.137465                                          #height of dune [m]
div= H/timedep_avgdepth                             #H/d
S= 0.0064                                           #slope from Run 12 of Fehlman [1985]
n=0.052915                                          #manning's coeff from Run 12 of Fehlman
                                                        [1985]
U= 1/n * timedep_avgdepth ^ (2/3) *S^(1/2)          #Manning's (Eqn 11)

i=1                                             #counter
hm=0                                            #establishing matrix

for (i in 1:length(t)) {
  if (div[i] <= .34) {
    hm[i]= 0.28* (U[i]^2)/(2*9.81) * ((div[i])/0.34)^(3/8)
} else
    hm[i]= 0.28* (U[i]^2)/(2*9.81) * ((div[i])/0.34)^(3/2)          #Eqn 12
}

lambda= H*6.7
normalized_h=c(-1,-.95,-0.8,-0.4,0.05,0.6,0.95,1,.85,0.55,0.3,-.35,-.8,-.95,-1,-1,-1,-1,-1)
                                                    #normalized_h is h/hm from Fig. 3

h_var=matrix(0,nrow=length(t),ncol=length(xcoord))      #h_dynamic [m]
h=matrix(0,nrow=length(t),ncol=length(xcoord))          #h_surface [m]


j=0                                             #counter
```

```
for (j in 1:length(xcoord)) {
  for (i in 1:length(t)) {
    h_var[i,j]=normalized_h[j]*hm[i]          #Eqn 13
    h[i,j]=h_var[i,j]+timedep_avgdepth[i]     #Eqn 14
  }
}

#All nodes export to tab-separated table
write.table(h,file="C:/Users/Documents/rdemo/input.txt", sep="\t")
```

B.2 Travel Time

```
modpath <- read.csv("1.0_0.91CL_gw.csv")          #read csv file of time-series of particle
                                                          locations into a matrix

travel<-numeric()                                 #this vector records travel time
particles<-numeric()                              #this vector keeps track of particles recorded

counter<-0

for (i in 2:(nrow(modpath)-1)) {                  #reading the appropriate column for location

  if (modpath[i,3]==modpath[(i-1),3] && modpath[i,3]==modpath[(i+1),3] ) {
                                                  #if particle location is the same for 3 timesteps
    if (counter == 0){                                    # records travel time for first particle
      counter<-counter+1

      travel[counter]= modpath[(i-2),5]           #then add its travel time to the matrix
      particles[counter]= modpath[(i-2),1]        #and record the particle number

    }else{
    if(modpath[i,1] != particles[counter]) {              # records travel time for all other particles

      counter<-counter+1

      travel[counter]= modpath[(i-2),5]           #then add its travel time to the matrix
      particles[counter]= modpath[(i-2),1]        #and record the particle number
    }
    }
  }
}


write.csv(travel,"travel.csv")
```

Appendix C: Benchmarking Results

Ran Basecase 3 from Hester et al. 2014 as a benchmark for the test. This basecase was chosen as it most closely replicated the surface water and groundwater conditions of this study (Table 3).

Table 6: Parameters used for Basecase 3.

Parameter	Units	Basecase 3
Hydraulic conductivity	m/d	84.4
Surface water DOC	mg/L	50
Groundwater DOC	mg/L	0
Surface water dissolved oxygen	mg/L	5
Groundwater dissolved oxygen	mg/L	0
Surface water nitrate	mg/L	0
Groundwater nitrate	mg/L	24.8

The results of the benchmark test matched those of reported values for the biodegradation of DOC, oxygen, and nitrate, seen in Hester et al. 2014 (Table 4). The smallest difference seen in the rate of consumption of the three solutes was that of NO_3. This is logical, because the nitrate is sourced from the groundwater upwelling at a constant flow. DOC and oxygen are sourced from the surface water. The minor differences in the biodegradation of these constituents is likely due to the slight difference in the surface water hydraulic head gradient originally used in Hester et al. 2014 and that generated by a script using equations developed in Elliott et al. 1997. The script-generated head distribution has a slightly larger range in values than that used in Basecase 3, resulting in a higher consumption of DOC and oxygen.

Table 7: Benchmark results compared to Basecase 3 results for biodegradation of DOC, oxygen, and nitrate.

	Solute consumed [mg/d]		
	DOC	DO	NO3
Benchmark run	93.2 (7.8%)	70.8 (59%)	44.9 (18%)
Basecase 3 (Hester et al. 2014)	84.2 (7.1%)	62.5 (53%)	42.8 (17%)

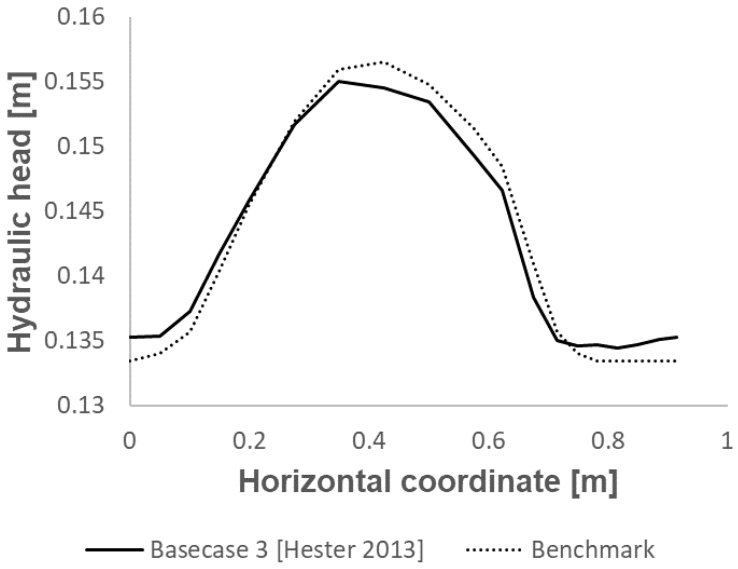

Figure 20: Comparison of head distributions implemented for Basecase 3 [*Hester et al*., 2014] and benchmark run.

Appendix D: Biodegradation Rate Calculations

D.1 Calculation for biodegradation rate using .OUT file from GMS

1. The .OUT file found in the SEAM3D folder generated for each model run gives cumulative mass budgets for each timestep.
2. Using the timesteps for 2.0 days and 1.0 days, one can calculate the biodegradation rate for all of the runs in this study, with the exception of the 48-hour run, which needs to be calculated from 0 to 2.0 days.
3. For example, by subtracting the mass biodegraded at 1 day from the mass biodegraded at 2 days one can get the mass biodegraded per day [mg/d].
    - In the case of the 48 hour run, one can take the total mass biodegraded at 2 days and divide by 2 days to find the average biodegradation per day.
    - Biodegradation Rate [mg/d] = ($Mass_{Bio\_T2}$ – $Mass_{Bio\_T1}$) / (T2-T1)
4. Calculating the rate of Cumulative $Mass_{in}$ worked much the same.
    - Cumulative $Mass_{in}$ [mg/d] = (Cumulative $Mass_{in\_T2}$ – Cumulative $Mass_{in\_T1}$) / (T2-T1)
5. To calculate the Percent Consumed, one would divide the Biodegradation rate by the Cumulative $Mass_{in}$.
    - Percent Consumed [%] = Biodegradation Rate [mg/d] / Cumulative $Mass_{in}$ [mg/d] *100%

D.2 Finding values in the .OUT file and sample calculations

- The .OUT file records each solute as Component No. 1, 2, 3… etc.
- For our model the components were as follows:
    - Component No. 1 = DOC Tracer
    - Component No. 2 = DO Tracer
    - Component No. 3 = NO3 Tracer
    - Component No. 4 = DOC
    - Component No. 5 = DO
    - Component No. 6 = NO3

```
>>>>>>>>>>>>>>>>>>>>>>>>>>>>>>>>>>>>>>>>>>>>>>>>>>>>>FOR COMPONENT NO. 06<<<<<<<<<<<<<<<<<<<<<<<<<<<<<<<<<<<<<<<<<<<<<<<<<<<<<<

                                          -----------------------------------------
                                                   TRANSPORT STEP NO. 2437
                                          -----------------------------------------

TOTAL ELAPSED TIME SINCE BEGINNING OF SIMULATION =    1.000000       d
...................................................................

                    CUMMULATIVE MASS BUDGETS AT END OF TRANSPORT STEP 2437, TIME STEP    1, STRESS PERIOD   10
                    ------------------------------------------------------------------------------------------

                                                 IN                           OUT
                                          ----------------             ----------------
                 CONSTANT CONCENTRATION:    0.000000                    0.000000
                          CONSTANT HEAD:   0.2949289E-04               -0.2283057
                                  WELLS:   0.2470600                    0.000000
                 DECAY OR BIODEGRADATION:   0.000000                   -0.1928838E-01
                   MASS STORAGE (SOLUTE):   0.1820236E-02              -0.1299205E-02
                 ---------------------------------------------------------------------------
                                [TOTAL]:   0.2489097        g          -0.2488933        g

                                          NET (IN - OUT):   0.1645088E-04
                                   DISCREPANCY (PERCENT):   0.6612483E-02
```

Figure 21: Cumulative mass budget at t = 1.0 d

```
>>>>>>>>>>>>>>>>>>>>>>>>>>>>>>>>>>>>>>>>>>>>>>>>>>>>>>FOR COMPONENT NO. 06<<<<<<<<<<<<<<<<<<<<<<<<<<<<<<<<<<<<<<<<<<<<<<<<<<<<<<

                                          -----------------------------------------
                                                   TRANSPORT STEP NO. 2439
                                          -----------------------------------------

TOTAL ELAPSED TIME SINCE BEGINNING OF SIMULATION =    2.000000       d
...................................................................

                    CUMMULATIVE MASS BUDGETS AT END OF TRANSPORT STEP 2439, TIME STEP    1, STRESS PERIOD   20
                    ------------------------------------------------------------------------------------------

                                                 IN                           OUT
                                          ----------------             ----------------
                 CONSTANT CONCENTRATION:    0.000000                    0.000000
                          CONSTANT HEAD:   0.5882903E-04               -0.4564971
                                  WELLS:   0.4941531                    0.000000
                 DECAY OR BIODEGRADATION:   0.000000                   -0.3843501E-01
                   MASS STORAGE (SOLUTE):   0.2234750E-02              -0.1724944E-02
                 ---------------------------------------------------------------------------
                                [TOTAL]:   0.4964467        g          -0.4966570        g

                                          NET (IN - OUT):  -0.2103448E-03
                                   DISCREPANCY (PERCENT):  -0.4235979E-01
```

Figure 22: Cumulative mass budget at t = 2.0 d

- Biodegradation Rate [mg/d] = ($Mass_{Bio\_T2}$ – $Mass_{Bio\_T1}$) / (T2-T1)
- Biodegradation Rate [mg/d] = (0.3843501e-01 g – 0.1928838e-01 g)/1.0 d *1000 mg/g
- Biodegradation Rate [mg/d] = 19.15 mg/d
- Cumulative $Mass_{in}$ [mg/d] = (Cumulative $Mass_{in\_T2}$ – Cumulative $Mass_{in\_T1}$) / (T2-T1)
- Cumulative $Mass_{in}$ [mg/d] = ((0.5882903e-04+0.4941531) – (0.2949289e-04+0.2470600)) / 1.0 d *1000 mg/g
- Cumulative $Mass_{in}$ [mg/d] = 247.12 mg/d
- Percent Consumed [%] = Biodegradation Rate [mg/d] / Cumulative $Mass_{in}$ [mg/d] *100%
- Percent Consumed [%] = (19.15 mg/d) / (247.12 mg/d) *100%
- Percent Consumed [%] = 7.75%

Appendix E: Additional Figures

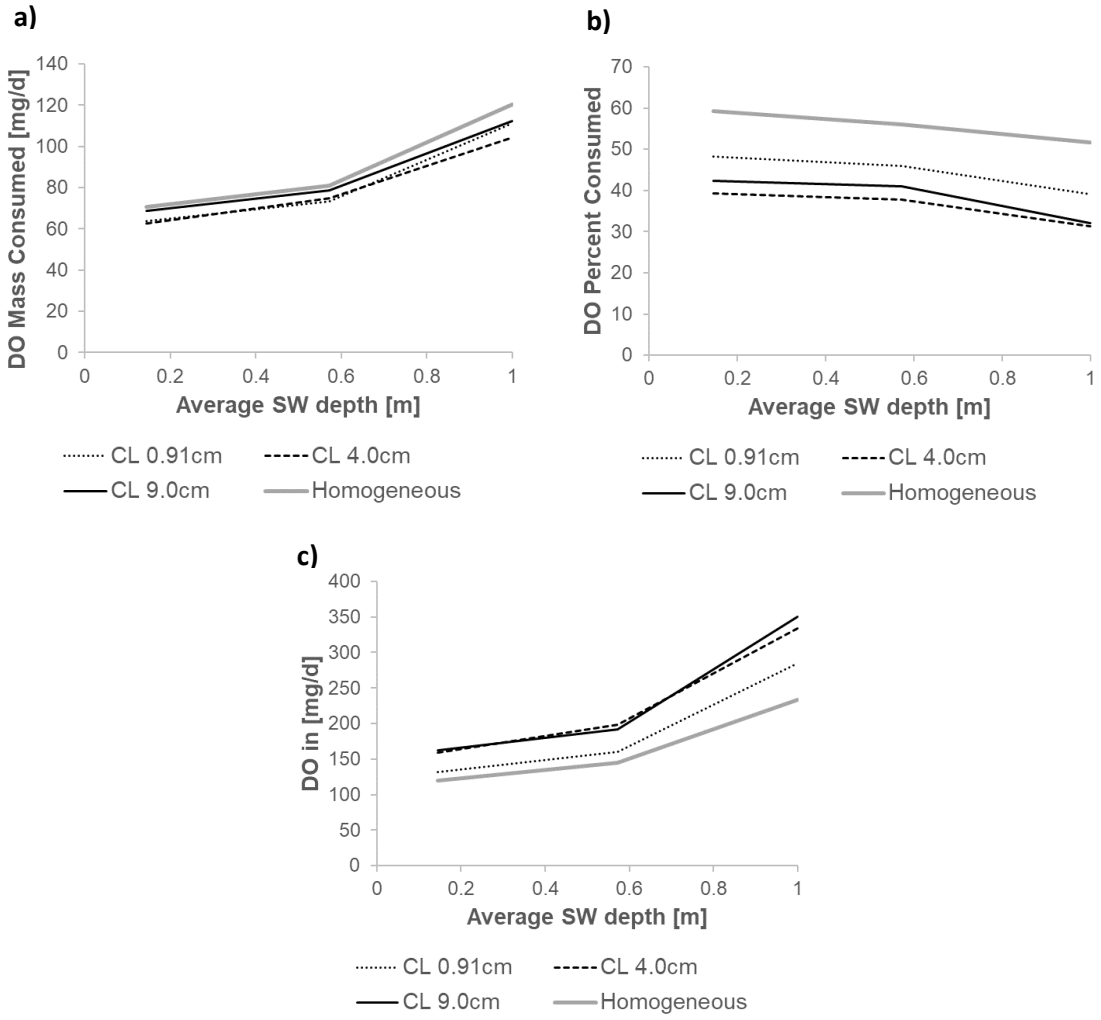

Figure 23: Alternative presentation of Figure 7. Comparison of a, b) non-mixing dependent aerobic respiration c) DO entering the dune from SW for a range of horizontal correlation lengths. These are steady-state runs on with varying average surface water depths. CL=heterogeneous hydraulic conductivity field horizontal correlation length, DO=dissolved oxygen, SW=surface water.

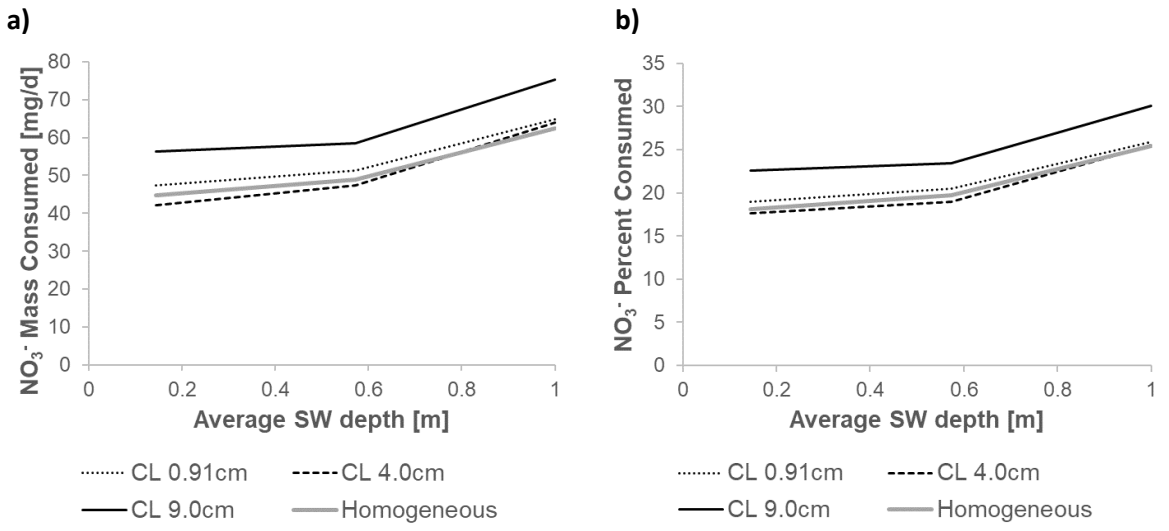

Figure 24: Alternative presentation of Figure 8. Comparison of mixing-dependent denitrification by a) mass consumed and b) percent of incoming nitrate undergoing reaction for a range of horizontal correlation lengths. These are steady-state runs on with varying average surface water depths. CL=heterogeneous hydraulic conductivity field horizontal correlation length, SW=surface water.

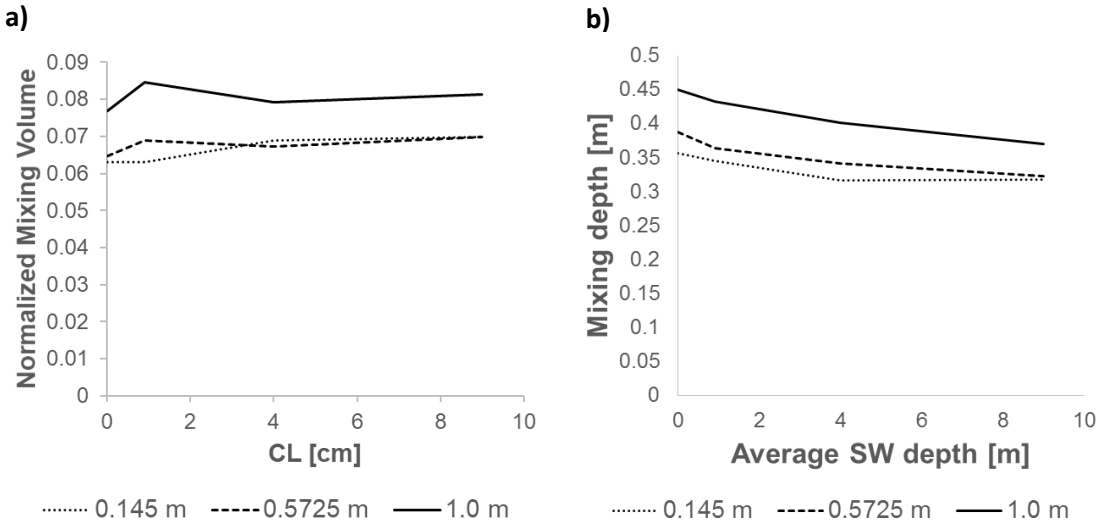

Figure 25: Trends in the a) normalized mixing zone volume and b) depth of the mixing zone for a series of correlation lengths. Mixing zone volume was measured using the NO3- tracer from the groundwater in the same way as Figure 2. Measuring the mixing zone depth was done by determining the deepest depth reached by tracer particles from the surface water and are reported as distanced from the peak of the dune. Normalized mixing volume was measured by the concentration gradient created by non-reactive tracers sourcing from the groundwater at the same concentrations as the reactive solute (NO_3^-). We defined the mixing zone volume as we did in Figure 15, normalizing to the model domain size. Homogeneous case is included as CL of zero.

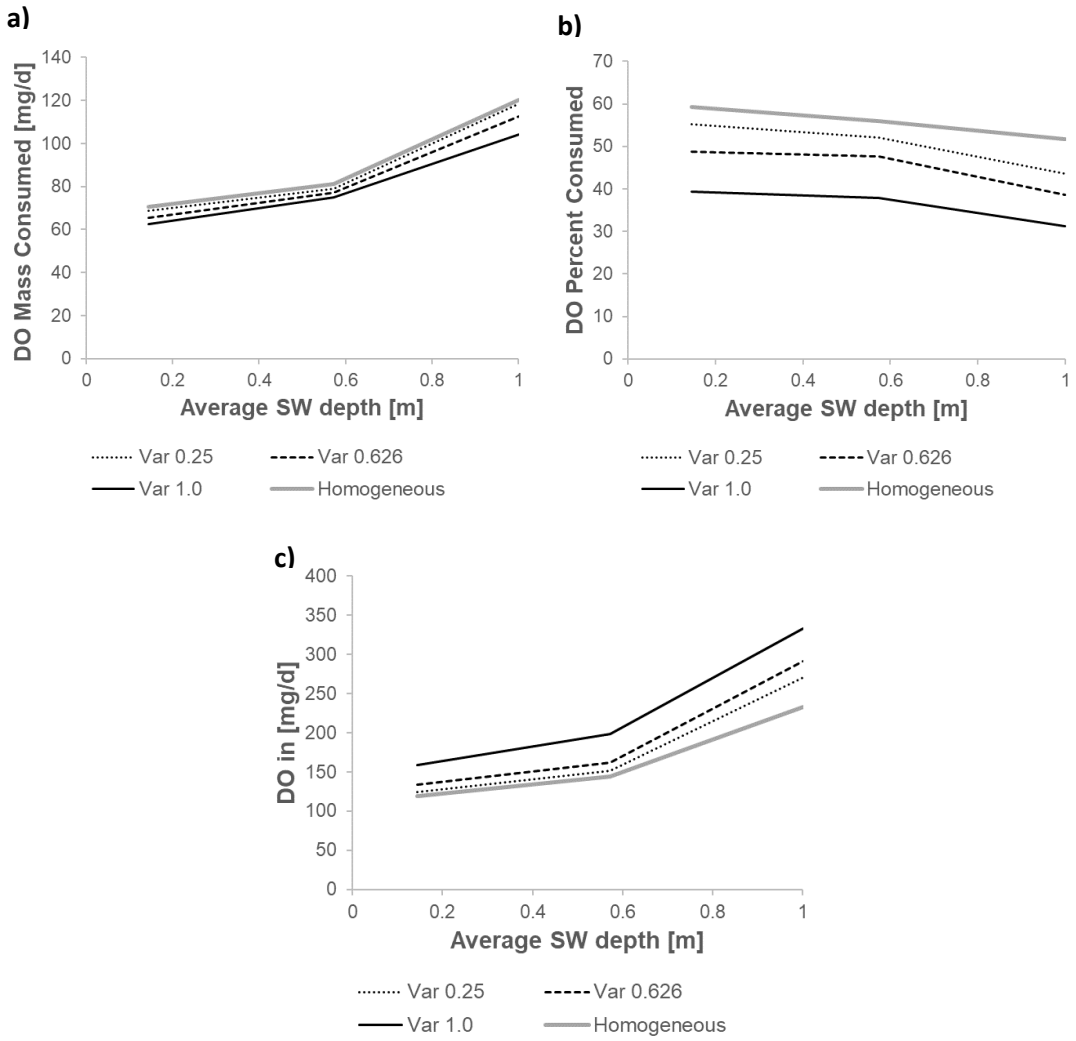

Figure 26: Alternative presentation of Figure 9. Comparison of a, b) non-mixing dependent aerobic respiration c) DO entering the dune from SW for a range of variances. These are steady-state runs on with varying average surface water depths. DO=dissolved oxygen, SW=surface water.

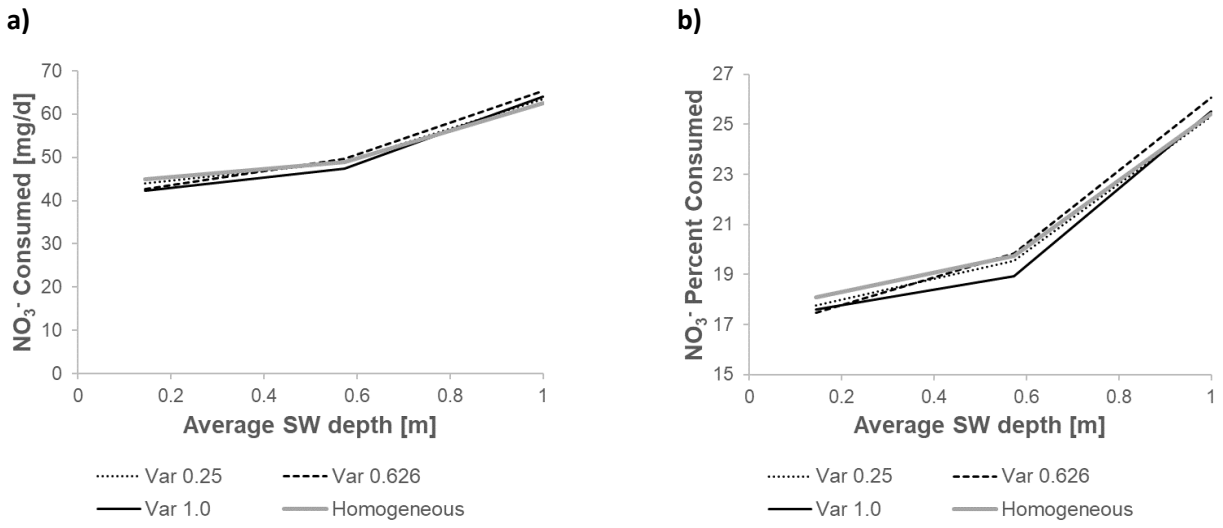

Figure 27: Alternative presentation of Figure 10. Comparison of mixing-dependent denitrification by a) mass consumed and b) percent of incoming nitrate undergoing reaction for a range of variances. These are steady-state runs on with varying average surface water depths. DO=dissolved oxygen, SW=surface water.

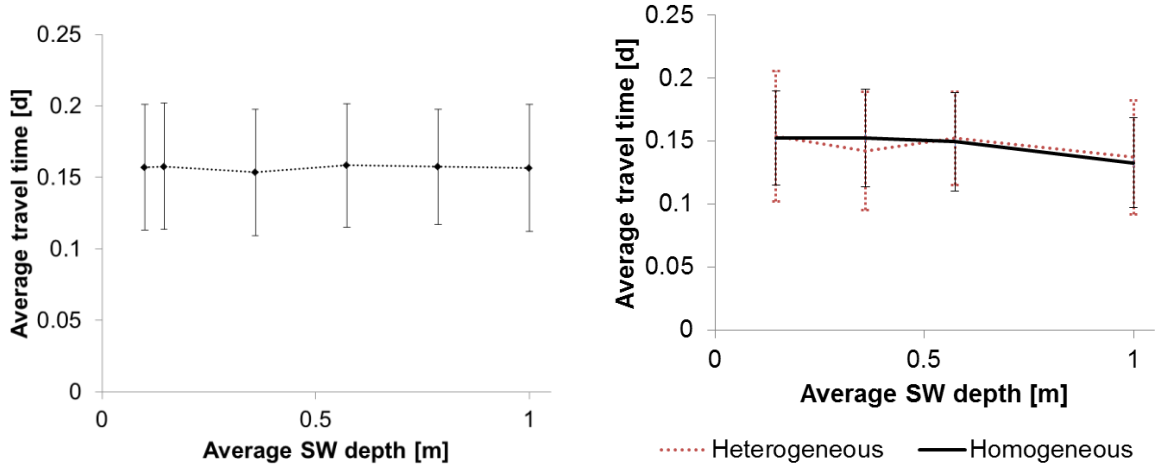

Figure 28: Average travel times for homogeneous case on a 25 m/d hydraulic conductivity field as in Figure 5. These are steady-state runs with varying average surface water depths. The depth of the stagnation point was measured by averaging the time it took for 45 tracer particles a standard distance directly under the deepest part of the mixing zone to reach the surface of the dune. The markers indicate the average travel time and error bars indicate the standard deviation of the particles.

Appendix F: Unsteady Heterogeneous Case

Running unsteady tests on heterogeneous field presented difficulties. The SEAM3D runtimes on these were extraordinary long (over 24 hours for the case that was run, a 12-hour transient fluctuation on the longest horizontal correlation length). Tests were attempted on higher variability fields, but these would not finish running in a reasonable timeframe.

SEAM3D uses a generated MODFLOW solution and looks at its complexity to determine an appropriate timestep to use to limit numerical dispersion. For the simplest tests run (steady-state, low SW depth, homogeneous field, 10 mm by 10 mm test grid), this timestep was on the order of e-05 and the model runtime would be ~1 hour. For the runs whose data are presented here (5 mm by 5 mm grid), the timestep was typically around e-06 and the model runtime would be roughly 10 hours. The magnitude of the timestep that SEAM3D uses approximately scales with the model runtime.

When attempting to run the unsteady case on heterogenous fields, the timestep that SEAM3D used was on the order of e-07. For the case that was run, that timestep was around 9e-07, so it did eventually finish. For the other cases, this timestep was closer to 1e-07. According to the scaling mentioned earlier, this would be approximately 100 hours of runtime. This problem was not only encountered in the unsteady case. In particular, for high variability heterogeneous fields, higher surface water depths had trouble running as well. As a result, the highest variability field tested was 1.0, the heterogeneous basecase for *Hester et al.* [2014].

Thoughts for future tests:

- Hyporheic exchange is induced by the pressure differential across the dune (i.e. the range in pressures).
- Early system tests indicated that adding a constant depth value of head across the entire dune had a negligible effect on the amount of biodegradation seen for DOC, DO and NO_3^-, even when that constant value was of significant magnitude (adding 0.5 m of head across the entire dune).
- *Elliott and Brooks* [1997] broke down the surface water head into a dynamic head and a static head, which combine to form a total head (Equations 13, 14).
- Since early tests showed that constant head values added across the entire dune had negligible impact, a case could potentially be built for neglecting the static head (equal to time-dependent depth) and only inputting the dynamic head as the specified head boundary condition in MODFLOW along the top of the dune.
- This should reduce the complexity of the MODFLOW hydraulic inputs for SEAM3D, reducing runtimes significantly.
- Alternatively, a coarser grid size could be used though tests of the numerical dispersion this presents would be necessary.

Appendix G: Sensitivity Coefficients

We calculated sensitivity coefficients using the following equation as seen in *Zheng and Bennett* [2002], also used in *Hester et al.* [2014].

$$X_{m,n} = \frac{\partial \hat{y}_m}{\partial\, a_n/a_n} \approx \frac{\hat{y}_m(a_n + \Delta a_n)}{\Delta a_n/a_n}$$

Where $X_{m,n}$ is the sensitivity coefficient of the dependent variable $\hat{y}$ with respect to the m^{th} parameter at the n^{th} observation point (in this case the mass consumed of NO_3^-), a_n is the parameter value for the basecase, Δa_n is the change in the parameter, and $\hat{y}(a_n)$ and $\hat{y}(a_n + \Delta a_n)$ are the values of the model-dependent variable obtained for the basecase and for the varied-parameter case, respectively. When evaluating the sensitivity coefficients for the heterogeneity parameters, the basecase value was considered to be that of the basecase parameter value with the same average surface water depth.

Table 8: Maximum sensitivity coefficients for parameters varied.

Parameter	**Unit**	*Steady-State Basecase*	*Amplitude Test Basecase*	*Transient Basecase*	*Heterogeneous Basecase*	**Maximum Sensitivity Coefficient (NO_3 consumed)**
Surface water boundary condition						
Depth	**m**	0.35875	0.5-0.7	0.145-1.0	-	9.18
Time-averaged depth (d_{avg})	**m**	-	0.6	0.5725	-	-
Amplitude	**m**	-	0.1	0.4275	-	0.33
Period	**hr**	-	24	24	-	0.89
Rate of change	**-**	-	sinusoidal	sinusoidal	-	-
Heterogeneous hydraulic conductivity						
Variance	**-**	-	-	-	1	6.03
Horizontal Correlation Length	**cm**	-	-	-	4	11.19